1   **Bmal1 integrates mitochondrial metabolism and macrophage activation**

2

3   Ryan K. Alexander[1], Yae-Huei Liou[1], Nelson H. Knudsen[1], Kyle A. Starost[1], Chuanrui Xu[1,2],

4   Alexander L. Hyde[1], Sihao Liu[1,3], David Jacobi[1,4], Nan-Shih Liao[5] and Chih-Hao Lee[1,*]

5

6   [1]Department of Molecular Metabolism, Division of Biological Sciences, Harvard T.H. Chan

7   School of Public Health, 665 Huntington Ave, Boston, MA 02115, USA

8   [2] School of Pharmacy, Tongji Medical College, Huazhong University of Science and

9   Technology, Wuhan, PR China

10   [3]Current address: Ionis Pharmaceuticals, 2855 Gazelle Ct, Carlsbad, CA 92110, USA

11   [4]Current address: l'institut du thorax, INSERM, CNRS, UNIV Nantes & CHU Nantes, Nantes,

12   France

13   [5]Institute of Molecular Biology, Academia Sinica, 128 Academia Rd. Section 2, Taipei, Taiwan,

14   ROC

15

16   *Correspondence should be addressed: C.-H.L. e-mail: clee@hsph.harvard.edu Department of

17   Molecular Metabolism, Harvard T.H. Chan School of Public Health, 665 Huntington Ave,

18   Bldg1, Rm 409, Boston, MA 02115, USA. Phone: +1(617) 432-5778

19

20

21   **ABSTRACT**

22   Metabolic pathways and inflammatory processes are under circadian regulation. While rhythmic

23   immune cell recruitment is known to impact infection outcomes, whether the circadian clock

24   modulates immunometabolism remains unclear. We find the molecular clock Bmal1 is induced by

25   inflammatory stimulants, including Ifn-γ/lipopolysaccharide (M1) and tumor conditioned medium,

26   to maintain mitochondrial metabolism under these metabolically stressed conditions in mouse

27   macrophages. Upon M1 stimulation, myeloid-specific *Bmal1* knockout (M-BKO) renders

28   macrophages unable to sustain mitochondrial function, enhancing succinate dehydrogenase

29   (SDH)-mediated mitochondrial ROS production and Hif-1α-dependent metabolic reprogramming

30   and inflammatory damage. In tumor-associated macrophages, the aberrant Hif-1α activation and

31   metabolic dysregulation by M-BKO contribute to an immunosuppressive tumor

32   microenvironment. Consequently, M-BKO increases melanoma tumor burden, while

33   administrating an SDH inhibitor dimethyl malonate suppresses tumor growth. Therefore, Bmal1

34   functions as a metabolic checkpoint integrating macrophage mitochondrial metabolism, redox

35   homeostasis and effector functions. This Bmal1-Hif-1α regulatory loop may provide therapeutic

36   opportunities for inflammatory diseases and immunotherapy.

37

2

INTRODUCTION

Inflammation and host defense are energetically costly processes that must balance the use of host resources with an efficient containment of infection or injury. This is underpinned by dynamic regulation of energy metabolism in immune cells in response to extrinsic signals, including cytokines, pathogen- and damage-associated molecular patterns and tumor-derived metabolites (Andrejeva & Rathmell, 2017; Buck, Sowell, Kaech, & Pearce, 2017; Ganeshan & Chawla, 2014; Hotamisligil, 2017; O'Neill, Kishton, & Rathmell, 2016). For instance, activation of macrophages by bacterial products, such as lipopolysaccharide (LPS) from gram-negative bacteria, shifts core metabolic function toward increased reliance on aerobic glycolysis with concomitant inhibition of mitochondrial respiration (Fukuzumi, Shinomiya, Shimizu, Ohishi, & Utsumi, 1996; Rodriguez-Prados et al., 2010; Tannahill et al., 2013). The depressed mitochondrial function appears to be by design, as this process serves multiple purposes. It leads to the so-called 'broken TCA cycle' due in part to shunting of citric acid to lipid synthesis (Andrejeva & Rathmell, 2017). Itaconate, also derived from citrate/aconitate, can modulate macrophage immune response through different mechanisms (Lampropoulou et al., 2016; Mills et al., 2018). By contrast, succinate accumulates through anaplerotic reactions, notably glutaminolysis (Tannahill et al., 2013). Succinate oxidation to fumarate mediated by succinate dehydrogenase (SDH)/ETC complex II activity is a primary source of mitochondrial reactive oxygen species (mROS) in inflammatory macrophages that are involved in bactericidal activity (Mills et al., 2016; West et al., 2011). Succinate/SDH is believed to trigger mROS production through accumulation of reduced coenzyme Q leading to reverse electron transfer to ETC complex I (Chouchani et al., 2014; Robb et al., 2018). These findings demonstrate a well-orchestrated metabolic signaling event at the expense of reduced fuel economy and compromised mitochondrial function in macrophages.

61   In addition to its bacterial-killing effect, mROS stabilize hypoxia-inducible factor (Hif) -

62 1α through inhibition of prolyl-hydroxylase enzymes that target Hif-1α for ubiquitination by the

63 von Hippel–Lindau (Vhl) E3 ubiquitin ligase and subsequent proteasomal degradation (Bell et al.,

64 2007; Jaakkola et al., 2001). Hif-1α is a master transcriptional regulator of genes involved in

65 glycolysis and anabolic metabolism, thereby supplementing the energetic needs of the broken TCA

66 cycle (Cramer et al., 2003; Masson & Ratcliffe, 2014; Semenza, Roth, Fang, & Wang, 1994). Hif-

67 1α is also required for the expression of the urea cycle enzyme arginase-1 (*Arg1*). Arg1 and nitric

68 oxide synthase 2 were initially designated as markers for M2 and M1 macrophages, as these two

69 enzymes convert amino acid arginine to citrulline and nitric oxide, respectively. However, M1

70 activation also up-regulates *Arg1* through Hif-1α. Similarly, in the nutrient-deprived tumor

71 microenvironment, tumor-derived lactate has been proposed to increase Hif-1α activity in tumor-

72 associated macrophages (TAMs) to up-regulate *Arg1* (Colegio et al., 2014). Aberrant expression

73 of Arg1 in TAMs results in local arginine depletion that inhibits antitumor immunity mediated by

74 cytotoxic T cells and natural killer (NK) cells (Doedens et al., 2010; Steggerda et al., 2017).

75 Accordingly, myeloid-specific deletion of *Hif1a* or *Arg1* suppresses tumor growth in mice

76 (Colegio et al., 2014; Doedens et al., 2010). These observations suggest that the distinction

77 between M1/M2 activation may not be as clear *in vivo* and highlight the importance of energetic

78 regulation in immune cell activation.

79   The circadian rhythm has been implicated in many biological/pathological processes,

80 including immune response and tumor progression (Hardin & Panda, 2013; Nguyen et al., 2013;

81 Papagiannakopoulos et al., 2016). The molecular clock includes the master regulator Bmal1 (or

82 Aryl hydrocarbon receptor nuclear translocator-like protein 1, Arntl) and its transcriptional partner

83 Clock as well as the negative regulatory loop, including Nr1d1, Nr1d2, period (Per1/2/3) and

4

84   cryptochrome (Cry1/2) proteins, and the positive regulator loop, including Rorα/β/γ (Hardin &

85   Panda, 2013). Several nuclear receptors, such as peroxisome proliferator-activated receptors,

86   Pparα, Pparδ/β and Pparγ, are downstream of Bmal1/Clock and control the expression of clock

87   output genes (Canaple et al., 2006; S. Liu et al., 2013; Yang et al., 2006). The circadian clock is

88   both robust and flexible. It has been demonstrated that time-restricted feeding in mice can

89   synchronize the peripheral clock separable from the central clock (Damiola et al., 2000),

90   suggesting that a primary function of circadian rhythm is to maximize the metabolic efficiency. In

91   concert, we and others have shown that hepatic Bmal1 regulates rhythmic mitochondrial capacity

92   in anticipation of nutrient availability (Jacobi et al., 2015; Peek et al., 2013). Prior studies have

93   implicated the circadian oscillator in regulating macrophage inflammatory function. Notably,

94   myeloid-specific *Bmal1* deletion disrupts diurnal monocyte trafficking and increases systemic

95   inflammation and mortality in sepsis mouse models (Nguyen et al., 2013). Whether and how the

96   circadian clock controls immune cell metabolism to modulate their effector functions remains

97   unclear.

98   In the present study, we describe a cell-autonomous role for Bmal1 in macrophage

99   energetic regulation. Bmal1 is induced following macrophage inflammatory stimulation. Its loss-

100   of-function exacerbates mitochondrial dysfunction, energetic stress and Hif-1α-dependent

101   metabolic reprogramming. By using the B16-F10 melanoma model, our results demonstrate that

102   the regulatory axis between Bmal1 and Hif-1α dictates macrophage energy investment that is

103   relevant for discrete activation/polarization states, including M1 and tumor-associated

104   macrophages.

105

106

107   **RESULTS**

108   **The circadian clock is a transcriptional module induced by M1 activation**

109   To assess transcriptional regulators that modulate macrophage energetics and inflammatory

110   function, we performed RNA sequencing (RNA-seq) comparing interferon-γ (Ifn-γ) primed bone

111   marrow-derived macrophages without or with LPS stimulation (10 ng/mL for 8 hours, referred to

112   as M1 activation). Gene ontology analysis using the DAVID platform was performed to identify

113   clusters of transcription factors that were up- or down-regulated in inflammatory macrophages,

114   which were used to generate a protein-protein interaction map using STRING (Figure 1

115   supplemental table 1 and Figure 1 supplemental figure 1A). Several activators of mitochondrial

116   function/biogenesis were repressed, including *c-Myc* (Li et al., 2005), *Pparg*, Pparg co-activator 1

117   beta (*Pgc1b*), and mitochondrial transcription factor B1 (*Tfb1m*) and *Tfb2m*. On the other hand,

118   the canonical inflammatory (e.g., *Nfkb1/2*, *Rela/b*, *Hif1a*, interferon regulatory factor 7 (*Irf7*) and

119   *Irf8*) and stress response (e.g., *Atf3*, *Atf6b* and *Nfe2l2*) transcriptional modules were up-regulated.

120   Interestingly, clusters of circadian oscillator components (e.g., *Per1*, *Cry1*, *Nr1d1*, *Nr1d2* and

121   *Rora*) as well as nuclear receptors downstream of the molecular clock (e.g., *Ppard* and its

122   heterodimeric partner *Rxra*) (S. Liu et al., 2013) were also induced.

123   We examined the expression of Bmal1, the non-redundant master regulator of circadian

124   rhythm, and found that M1 activation (Figure 1A) or LPS treatment without Ifn-γ priming (Figure

125   1B) induced its mRNA and protein levels, peaking at 12 hours after the stimulation. Because LPS

126   was directly added to the cell culture without changing the medium, the induction of Bmal1 was

127   not due to serum shock (Tamaru et al., 2003). In fact, a one-hour LPS treatment in culture medium

128   with 2% serum was sufficient to reset Bmal1 expression (Figure 1C), in a manner resembling

129   serum shock (requiring a much higher serum concentration). Similar results were observed in

130   mouse embryonic fibroblasts (MEFs), suggesting that the inflammatory regulation of Bmal1 was

131   not macrophage-specific (Figure 1 supplemental figure 1B).

132   Myeloid-specific *Bmal1* knockout (M-BKO, *Bmal1f/f* crossed to *Lyz2-Cre*; *Bmal1f/f* was

133   used as the wild-type control, WT) mice were generated to determine the role of circadian clock

134   in macrophage function. M-BKO did not affect M1 induction of canonical inflammatory

135   regulators, such as *Nfkb1*, *Stat3*, *Hif1a* and *c-Myc* (Figure 1D). The expression of genes

136   downstream of Bmal1, including *Nr1d2*, *Cry1* and *Ppard*, was dysregulated, and there was a

137   further reduction of *Pparg* expression by M1 activation in M-BKO macrophages compared to WT

138   cells (Figure 1D). By contrast, M2 activation by Il-4 did not regulate *Bmal1* mRNA levels, and Il-

139   4-induced expression of *Arg1* and *Mgl2* was not altered by M-BKO (Figure 1 supplemental figure

140   1C). These results suggest that the circadian clock may function as a downstream effector of M1

141   stimulation in a cell-autonomous manner.

142

Bmal1 promotes mitochondrial metabolism in inflammatory macrophages

144   Because Pparδ/Pparγ are known regulators of mitochondrial function and energy substrate

145   utilization in macrophages (Dai et al., 2017; Kang et al., 2008; Lee et al., 2006; Odegaard et al.,

146   2007), we sought to determine the role of Bmal1 in macrophage bioenergetic control. In WT

147   macrophages, M1 activation caused a progressive decrease in mitochondrial content, which was

148   more pronounced in M-BKO macrophages (Figure 2A). The reduced mitochondrial content was

149   likely due to mitophagy, as demonstrated by the increased level of the mitophagy receptor Bnip3

150   (Figure 2B). Measurement of ETC complex activity in isolated mitochondria indicated that M-

151   BKO also caused a significant reduction in the activities of complex II and III, given an equal

152   amount of mitochondrial protein, 6 hours after M1 stimulation (Figure 2C). Seahorse extracellular

153   flux analysis showed that LPS injection increased the extracellular acidification rate (ECAR,

154   indicative of lactic acid secretion) and decreased the oxygen consumption rate (OCR) of WT

155   macrophages, as expected from aerobic glycolysis (Figure 2D). The ECAR and OCR were further

156   enhanced and suppressed, respectively, in M-BKO macrophages. Similar results were obtained in

157   thioglycollate-elicited peritoneal macrophages isolated from WT and M-BKO mice (Figure 2

158   supplemental figure 1A). By contrast, stable overexpression of *Bmal1* (Bmal1-OE) in RAW264.7

159   macrophages resulted in a higher OCR and lower ECAR after LPS stimulation, compared to

160   control cells (Figure 2 supplemental figure 1B-C). To directly examine aerobic glycolysis, glucose

161   was injected during the extracellular flux assay with or without co-injection with LPS. There was

162   no difference in the basal glycolytic rate between WT and M-BKO macrophages (Figure 2E). LPS

163   increased ECAR in both genotypes and to a greater extent in M-BKO macrophages. The induced

164   ECAR could be blocked by injection of 2-deoxyglucose (2-DG), confirming the acidification was

165   caused by aerobic glycolysis. Furthermore, an increase in the glycolytic rate was observed in

166   splenic macrophages from M-BKO mice isolated 6 hours after *i.p.* injection of LPS, which was

167   accompanied by lowered circulating glucose levels, indicative of increased glucose consumption

168   by inflammatory myeloid cells in M-BKO mice, compared to WT animals (Figure 2 supplemental

169   figure 1D-E).

170   To further assess the metabolic state, metabolomics analyses were employed to compare

171   cellular metabolite levels of WT and M-BKO macrophages 0, 6 and 12 hours after M1 activation

172   (Figure 3A-B and Figure 3 supplemental table 1). As has been reported (Tannahill et al., 2013),

173   M1 activation caused accumulation of glycolytic intermediates (glucose-6-phosphate, fructose-6-

174   phosphate and lactic acid) and depletion of TCA metabolites (e.g. citrate) but accumulation of

175   succinate. Glycolytic metabolites and succinate were significantly higher in M-BKO macrophages

176 compared to WT cells. M-BKO cells also showed accumulation of several amino acids and

177 intermediates of the urea cycle (which detoxifies ammonia released from amino acid deamination)

178 (Figure 3A and Figure 3 supplemental table 1). Consistent with the increased glycolytic

179 metabolites, M1-stimulated glucose uptake and lactate production were higher in M-BKO

180 macrophages (Figure 3C-D). These results suggest *Bmal1* loss-of-function leads to metabolic

181 dysregulation in M1-stimulated macrophages.

182

183 **The Bmal1-Hif-1α crosstalk regulates macrophage energy metabolism**

184 As mentioned earlier, Hif-1α is a primary regulator of glucose metabolism in inflammatory

185 macrophages. The enhanced aerobic glycolysis in M-BKO macrophages prompted us to examine

186 whether Hif-1α activity was aberrantly elevated. Western blot analyses revealed that M1 activation

187 led to a several-fold induction of Hif-1α protein levels in M-BKO macrophages compared to WT

188 cells (Figure 4A), while Bmal1-OE RAW264.7 macrophages showed reduced Hif-1α protein

189 (Figure 4 supplemental figure 1A). The expression of Hif-1α targets, such as lactate

190 dehydrogenase A (*Ldha*), *Arg1* and *Il1b*, was enhanced by M-BKO and blocked by myeloid *Hif1a*

191 knockout (M-HKO, Figure 4B). Hif-1α gene expression was not different between WT and M-

192 BKO cells (Figure 1D). mROS derived from increased succinate oxidation has previously been

193 demonstrated to stabilize Hif-1α protein in inflammatory macrophages (Mills et al., 2016).

194 Metabolite analyses showed accumulation of succinate in M-BKO macrophages, suggesting that

195 elevated mROS may be the cause of the increased Hif-1α protein. In fact, levels of mROS were

196 higher in isolated mitochondria from M-BKO macrophages at 1 and 4 hours of M1 activation

197 compared to WT macrophages (Figure 4C). Addition of succinate increased mROS production in

198 mitochondria from both WT and M-BKO macrophages. An additional two-fold induction of

9

199 mROS was detected in mitochondria from 4-hour M1 stimulated M-BKO, but not WT

200 macrophages. Hif-1α protein accumulation could be normalized between genotypes by co-

201 treatment with the antioxidant N-acetylcysteine (N-AC) or the competitive complex II inhibitor

202 dimethylmalonate (DMM) that blocks mROS production (Figure 4D). Furthermore, M1-

203 stimulated glucose uptake, lactate release and aerobic glycolysis were attenuated in myeloid-

204 specific *Bmal1* and *Hif1a* double knockout macrophages (M-BHdKO, Figure 4 supplemental

205 figure 1B-D), indicating the increased glucose utilization in M-BKO was Hif-1α-dependent.

206 A previous study suggests that *Bmal1* deletion impairs the expression of *Nfe2l2* (which

207 encodes Nrf2) and its downstream antioxidant genes thereby increasing oxidative stress (Early et

208 al., 2018). However, we found that expression *Nfe2l2* and Nrf2-induced oxidative stress responsive

209 genes, such as NAD(P)H quinone dehydrogenase 1 (*Nqo1*, Figure 4 supplemental figure 1E), were

210 up-regulated in M-BKO macrophages upon M1 stimulation, suggesting that increased mROS

211 associated with M-BKO was the cause rather than consequence of dysregulated Nrf2 signaling.

212 Collectively, these data indicate that Bmal1 and Hif-1α regulate opposing metabolic programs and

213 that Bmal1-mediated mitochondrial metabolism serves to fine-tune Hif-1α activity by modulating

214 oxidative stress.

215

216 ***Bmal1* loss-of-function induces metabolic reprogramming toward amino acid catabolism**

217 To fully characterize metabolic programs that were impacted by *Bmal1* loss-of-function,

218 we compared RNA-seq data from control and M1-activated WT and M-BKO macrophages. These

219 analyses revealed that the majority of M1-induced or suppressed genes were regulated in a similar

220 manner between WT and M-BKO macrophages, suggesting that *Bmal1* gene deletion did not cause

221 a general defect in inflammatory activation (Figure 5 supplemental figure 1A and Figure 5

10

222   supplemental table 1). Gene ontology analyses of the top enriched categories of M1-upregulated

223   genes shared by both genotypes included regulation of apoptosis, response to stress and cytokine

224   production. Among the top categories of suppressed genes were the cell cycle, DNA repair and

225   carbohydrate metabolism. The latter showed that most TCA cycle enzymes were down-regulated

226   by M1 activation (Figure 5A).

227   Direct comparison between M1-stimulated WT and M-BKO macrophages revealed that

228   genes more highly expressed in M1-activated M-BKO macrophages were enriched for protein

229   catabolism and amino acid transport (Figure 5 supplemental figure 1B and Figure 5 supplemental

230   table 1). These included genes encoding plasma membrane amino acid transporters (e.g., *Slc7a2*,

231   *Slc7a8*, *Slc7a11*, *Slc38a2* and *Slc38a7*) as well as ubiquitin-activating, -conjugating and -ligating

232   enzymes that target proteins for proteasomal degradation (e.g., ubiquitin-like modifier-activating

233   enzyme 6 (*Uba6*), ubiquitin conjugating enzymes *Ube2q2* and *Ube2e3*, ring finger proteins *Rnf12*,

234   *Rnf56*, *Rnf128*, and *Rnf171*, cullin 3 (*Cul3*) and *Cul5*, and ubiquitin protein ligase e3a (*Ube3a*))

235   (Figure 5A-B). The expression of enzymes involved in the breakdown of branched chain amino

236   acids was also higher in M1-activated M-BKO cells, including branched chain keto acid

237   dehydrogenase E1 subunit beta (*Bckdhb*) and methylmalonate semialdehyde dehydrogenase

238   (*Mmsdh*). These results are consistent with increased amino acid catabolism observed in metabolite

239   assays (Figure 3A). Interestingly, certain genes described above, notably *Slc7a8*, appeared to be

240   counter-regulated by Hif-1α, as their induction by M1 stimulation was blunted in M-HKO

241   macrophages (Figure 5 supplemental figure 1C).

242   Slc7a8, also called L-type amino acid transporter 2 (Lat2), transports neutral amino acids

243   that could be converted to succinate and potentially contribute to Hif-1α protein stabilization. In

244   line with increased amino acid metabolism, extracellular flux analysis showed that M-BKO

245 macrophages showed enhanced glutamine utilization compared to WT cells, which was blocked

246 by 2-amino-bicyclo-(2,2,1)-heptane-2-carboxylate (BCH), an L-type amino acid transporter

247 inhibitor (Christensen, Handlogten, Lam, Tager, & Zand, 1969; Segawa et al., 1999) (Figure 5

248 supplemental figure 1D). BCH decreased and normalized levels of Hif-1α protein between WT

249 and M-BKO macrophages (Figure 5C). In addition, treatment with either BCH or DMM

250 suppressed the expression of *Il1b*, *Slc7a8* and *Slc7a11* induced by M1 stimulation (Figure 5D).

251 The combination of BCH and DMM did not exert a greater effect over that of DMM alone. Thus,

252 amino acid metabolism is up-regulated in response to dysregulated energy metabolism in M-BKO

253 macrophages, which contributes to increased oxidative stress and Hif-1α activation.

254

255 **Macrophage *Bmal1* gene deletion promotes an immune-suppressive tumor-associated**

256 **macrophage phenotype and enhances tumor growth**

257 It has been suggested that myeloid-specific *Bmal1* deletion disrupts diurnal monocyte

258 trafficking thereby increasing sepsis-induced systemic inflammation and mortality (Nguyen et al.,

259 2013). Our results suggest that the cell-autonomous function of Bmal1 on macrophage metabolism

260 and Hif-1α activation may contribute to the reported phenotype. Hif-1α regulates the polarization

261 of M1 and tumor-associated macrophages, both of which are under energetically challenged

262 conditions. We sought to determine whether the Bmal1-Hif-1α crosstalk plays a role in modulating

263 TAM activation through a mechanism similar to that in M1 stimulation. Treatment of macrophages

264 with conditioned medium from primary B16-F10 tumors (T-CM) increased the expression of

265 *Bmal1* mRNA as well as protein (Figure 6A). M-BKO macrophages showed enhanced mROS

266 production and Hif-1α protein induced by T-CM, compared to WT macrophages (Figure 6B-C).

267 Tracking with Hif-1α stabilization, aerobic glycolysis was up-regulated by T-CM pretreatment in

268   WT and to a greater extent in M-BKO macrophages (Figure 6D). T-CM elicited an energetic stress

269   gene expression signature resembling M1 stimulation, including up-regulated amino acid

270   metabolism (*Arg1*, *Slc7a8* and *Bckdhb*) and oxidative stress (*Slc7a11* and *Nqo1*) pathways in WT

271   macrophages that were further induced by M-BKO (Figure 6E). Subsequently, we employed a

272   mouse model of melanoma through subcutaneous injection of B16-F10 melanoma cells to assess

273   the impact of myeloid *Bmal1* deletion on tumor growth. Tumor volume was increased in both male

274   and female M-BKO mice compared to WT controls (Figure 6F). Furthermore, the expression of

275   *Arg1*, *Slc7a8* and *Slc7a11* was up-regulated in F4/80$^+$ cells isolated from tumors but not spleens

276   of M-BKO mice compared to WT animals (Figure 6G). Of note, the mRNA levels of *Arg1*, *Slc7a8*

277   and *Slc7a11* were substantially higher in tumor versus splenic F4/80$^+$ cells, consistent with the

278   results observed in T-CM treated macrophages.

279   To confirm that macrophage Bmal1 modulates tumor growth cell-autonomously and assess

280   the effect of TAMs on anti-tumor immune response within the same host environment, we co-

281   injected B16-F10 cells with either WT or M-BKO macrophages into the right or left flanks,

282   respectively, of WT mice. Tumor growth rate was substantially higher when co-injected with M-

283   BKO macrophages compared to WT cell co-injection (Figure 7A). In concert, co-injection with

284   M-BKO macrophages led to a reduction in the CD8$^+$ T cell population among tumor-infiltrating

285   CD45$^+$ leukocytes as well as functionally primed CD8$^+$ T and NK cells that expressed Ifn-γ protein

286   following stimulation with phorbol myristate acetate and ionomycin *ex vivo* (Figure 7B). Similar

287   results were obtained when the co-injections were performed in M-BKO mice (Figure 7

288   supplemental figure 1A-B).

289   We next sought to address the importance of oxidative stress in TAM activation. Similar

290   to M1 macrophages, DMM blocked Hif-1α protein accumulation and attenuated *Arg1* up-

291   regulation in T-CM-treated macrophages (Figure 7 supplemental figure 1C-D). Administering

292   DMM (~150 mg/kg body) at the time of macrophage-tumor cell co-inoculation effectively

293   suppressed melanoma tumor growth and normalized the difference in tumor promoting effects

294   between WT and M-BKO macrophage (Figure 7C). These results reveal a unifying mechanism

295   through which Bmal1 controls macrophage effector functions through bioenergetic regulation and

296   suggest that targeting oxidative stress may provide a means to modulate the anti-tumor activity of

297   TAMs.

298

299

300 **DISCUSSION**

301   It has been reported that sepsis exerts a long-lasting effect on circadian rhythm alteration

302 in mice (Marpegán, Bekinschtein, Costas, & Golombek, 2005; O'Callaghan, Anderson, Moynagh,

303 & Coogan, 2012). In the current study, we show that inflammatory stimulants, including Ifn-γ/LPS

304 and tumor-derived factors, control the expression of the circadian master regulator Bmal1 in the

305 macrophages. Our data further demonstrate that Bmal1 is an integral part of the metabolic

306 regulatory network and modulates macrophage activation, in part, through crosstalk with Hif-1α.

307 The Bmal1-Hif-1α regulatory loop regulates the balance between oxidative and glycolytic

308 metabolism in energetically stressed macrophages with distinct effector functions. *Bmal1* loss-of-

309 function in M1-activated macrophages causes mitochondrial dysfunction, thereby potentiating

310 mROS production and Hif-1α protein stabilization, which likely contributes to the increased

311 sepsis-induced inflammatory damage reported for M-BKO mice (Nguyen et al., 2013). Within the

312 tumor microenvironment, macrophage *Bmal1* gene deletion leads to compromised anti-tumor

313 immunity and accelerated tumor growth in a mouse melanoma model. Therefore, the Bmal1-Hif-

314 1α nexus serves as a metabolic switch that may be targeted to control macrophage effector

315 functions.

316   Much attention has been focused on how inflammatory stimuli disrupt mitochondrial

317 metabolism as a means to generate signaling molecules, including TCA metabolites and mROS.

318 The analysis of transcriptional modules involved in macrophage inflammatory response reveals a

319 coordinated effort in the control of mitochondrial activity. The expression of several regulators of

320 mitochondrial biogenesis (e.g., *Pparg*) is down-regulated rapidly after M1 stimulation and

321 rebounds between 8-12 hours, when *Bmal1* and *Ppard* expression are induced (Figure 1). Several

322 lines of evidence indicate that Bmal1 plays a key role in restoring mitochondrial function and in

15

323   modulating Hif-1α-mediated inflammatory response. The expression of transcription factors

324   known to control mitochondrial bioenergetics discussed above (i.e., Pparγ and Pparδ) is down-

325   regulated by M-BKO. Macrophages deficient in *Bmal1* are unable to sustain mitochondrial

326   function upon M1 stimulation, while Bmal1 gain-of-function in RAW 246.7 macrophages

327   promotes oxidative metabolism. The metabolic dysregulation in M-BKO macrophages further

328   promotes Hif-1α-controlled glycolytic metabolism and other alternative sources for fuel

329   utilization, such as amino acid catabolism. Although Bmal1 is best known for its role in circadian

330   regulation and has been shown to control rhythmic monocyte recruitment and gene expression

331   (Nguyen et al., 2013), our data suggest that LPS or M1 stimulation could "reset the clock" by

332   inducing/resynchronizing the expression of *Bmal1*. In this context, Bmal1 controls the timing of

333   glycolytic to oxidative metabolism transition that dictates the extent of Hif-1α activation and the

334   associated inflammatory response.

335   Both Bmal1 and Hif-1α belong to the basic helix-loop-helix (bHLH) transcription factor

336   family and have similar domain structures. However, they appear to regulate opposing metabolic

337   programs, with Hif-1α serving as a master regulator of aerobic glycolysis and Bmal1 as a positive

338   regulator of oxidative metabolism (Figure 7 supplemental figure 1E). The crosstalk between these

339   two bHLH transcription factors is in part mediated by succinate and SDH/complex II-facilitated

340   mROS production. Succinate is one of the entry points for anerplerosis that attempts to replenish

341   TCA cycle metabolites depleted by disruption of mitochondrial oxidative metabolism. Increased

342   protein/amino acid catabolism provides a source of anerplerotic reactions. Succinate accumulation

343   and the subsequent oxidation to fumarate, however, generate mROS, which stabilizes Hif-1α

344   protein to drive aerobic glycolysis. Our data suggest that amino acid metabolism appears to be

345   down- and up-regulated by Bmal1 and Hif-1α, respectively, as demonstrated by the regulation of

346   *Arg1* and *Slc7a8* gene expression. Hif-1α has also been shown to regulate Bnip3-mediated

347   mitophagy that reduces mitochondrial oxidative capacity (Zhang et al., 2008). Therefore, Bmal1-

348   controlled mitochondrial metabolism provides a break to this feedforward cycle to limit

349   inflammatory damage. In line with this, previous work has demonstrated that myeloid *Bmal1*

350   knockout mice have reduced survival rate upon *L. monocytogenes* infection (Nguyen et al., 2013).

351   These observations indicate a tightly regulated metabolic program in the macrophage to execute

352   effector functions and place Bmal1-regulated mitochondrial metabolism at the center of an orderly

353   and balanced immune response.

354   Despite being characterized as M2-like, TAMs share several common features with M1-

355   activated macrophages. Both of them function under nutrient-restricted conditions and Hif-1α is

356   required for their activation. Previous studies implicate a glycolytic preference of TAMs in breast,

357   thyroid, and pancreatic cancer (Arts et al., 2016; D. Liu et al., 2017; Penny et al., 2016). Our data

358   confirm that T-CM treatment enhances glycolysis in the macrophage accompanied by increased

359   Hif-1α protein (Figure 6C-D). *Arg1*, originally defined as an M2 marker, is a *bona fide* target of

360   Hif-1α up-regulated in TAMs and M1 macrophages. Arg1 is involved in the urea cycle that

361   detoxifies ammonia, and its induction supports amino acid catabolism. M-BKO macrophages show

362   increased mROS, glycolytic metabolism and Hif-1α stabilization and up-regulation of *Arg1* and

363   *Slc7a8* upon treatment with T-CM. Dysregulated amino acid metabolism has been shown to impact

364   immune cell activation. Arginine depletion impairs lymphocyte function, as arginine is required

365   for effector T cell and NK cell proliferation and maintenance (Geiger et al., 2016; Lamas et al.,

366   2012; Steggerda et al., 2017). Slc7a8 transports neutral amino acids, including branched chain

367   amino acids that are essential for lymphocyte activation and cytotoxic function (Sinclair et al.,

368   2013; Tsukishiro, Shimizu, Higuchi, & Watanabe, 2000). As such, the increased amino acid

17

369   utilization by M-BKO macrophages may contribute to the observed reduction in populations of

370   Ifn-γ-producing CD8$^+$ T and NK cells in tumor-infiltrating CD45$^+$ leukocytes (Figure 7B and

371   Figure 7 supplementary figure 1B). The fact that amino acid/protein metabolism and oxidative

372   stress genes (*Arg1*, *Slc7a8* and *Slc7a11*) are up-regulated in TAMs, compared to splenic

373   macrophages (Figure 6G) supports the notion that the energetic stress is also a key determinant of

374   TAM polarization. As a proof-of-principle approach, we show that DMM treatment blocks T-CM

375   induced Hif-1α protein stabilization *in vitro* and suppresses tumor growth *in vivo*. Thus, while M1

376   macrophages opt for an inefficient way to produce ATP, TAMs are limited in energy allocations.

377   Both of these processes result in an energetically challenged state in which Bmal1-Hif-1α crosstalk

378   controls the metabolic adaptation that shapes macrophage polarization. Future studies

379   investigating mechanisms to harness this energetic stress will likely identify means to effectively

380   modulate immune cell functions.

381

382

383 **MATERIALS and METHODS**

384 **Reagents.** Lipopolysaccharide, or LPS, from *Escherichia coli* strain K-235 (L2143) was from

385 Sigma-Aldrich. Recombinant murine Ifn-γ (315-05) and Il-4 (214-14) were from Peprotech. The

386 ETC complex II inhibitor dimethyl malonate (136441) and the L-type amino acid transport

387 inhibitor 2-amino-2-norbornanecarboxylic acid, or BCH, (A7902) were from Sigma-Aldrich.

388

389 **Animals**. All animal studies were approved by the Harvard Medical Area Standing Committee on

390 Animal Research. Animals were housed in a pathogen-free barrier facility at the Harvard T.H.

391 Chan School of Public Health. *Bmal1$^{fl/fl}$* (stock # 007668), *Hif1a$^{fl/fl}$* (stock # 007561), and *Lyz2-*

392 *Cre* (stock # 004781) mice in the C57BL/6J background were obtained from Jackson lab and were

393 originally contributed by Drs. Charles Weitz, Dmitriy Lukashev, and Irmgard Foerster,

394 respectively. Floxed mice were crossed with *Lyz2-Cre* mice to generate myeloid-specific *Bmal1*

395 and *Hif1a* knockout mice. Myeloid-specific *Bmal1* knockout mice were crossed with *Hif1a$^{fl/fl}$*

396 mice, and the resulting heterozygotes were crossed to generate myeloid-specific *Bmal1* and *Hif1a*

397 double knockout mice. The genotypes were validated by both DNA genotyping and mRNA

398 expression. Gender- and age-matched mice between 8-24 weeks of age were used for experiments.

399 Similar results were obtained from male and female mice.

400

401 **Bone marrow-derived macrophage (BMDM) differentiation and cell culture.** Macrophages

402 were differentiated from primary mouse bone marrow from the femur and tibia using

403 differentiation medium containing 30% L929-conditioned medium, 10% FBS, and pen-strep

404 solution in low-glucose DMEM in 15 cm petri dishes. Media were changed every three days, and

405 cells were lifted, counted, and plated in final format in tissue culture plates on days 7-8 of

406   differentiation. For experiments, primary macrophages were maintained in low glucose DMEM

407   containing 10% FBS and pen-strep. For M1 activation, macrophages were primed with 10 ng/mL

408   Ifn-γ for 10-12 hours and subsequently stimulated with 10 ng/mL of *E. coli* LPS at the start of each

409   experiment. Macrophages with Ifn-γ priming but without LPS were used as the control for M1

410   activation.

411

412   **Peritoneal and splenic macrophage isolation and culture.** For peritoneal macrophage isolation,

413   mice aged 2-4 months were *i.p.* injected with 3 mL of 3% thioglycollate (Sigma-Aldrich, T9032).

414   After 3 days, mice were euthanized, and peritoneal cells were recovered by lavage. For isolation

415   of splenic macrophages, mice were euthanized and spleens were dissected and mashed in growth

416   medium (high glucose DMEM with 10% FBS) and passed through a 70 μm strainer. Cells were

417   pelleted and resuspended in red blood cell lysis buffer. Monocytes and lymphocytes were

418   recovered using the Ficoll-Paque Plus density gradient medium (GE Healthcare Life Sciences,

419   17144002) according to the manufacturer's instructions, and suspension cells (lymphocytes) were

420   washed away prior to experiments.

421

422   **LPS synchronization of Bmal1 expression.** To synchronize Bmal1 gene and protein expression

423   with LPS (or LPS shock), BMDMs or MEFs were given fresh culture medium with 2% FBS and

424   100 ng/mL LPS for 1 hour and then given fresh medium with 2% FBS without LPS. Bmal1

425   expression was tracked following LPS removal. For M1 or LPS induction of Bmal1 expression,

426   cells were primed with or without 10 ng/mL Ifn-γ for 10-12 hours in DMEM, 10% FBS and

427   subsequently stimulated with 10 ng/mL of LPS without changing the medium (time zero).

428

429   **Cell lines.** Mouse embryonic fibroblasts (MEFs) were isolated from WT C57/BL6J mouse

430   embryos and immortalized using the 3T3 protocol as previously described(Xu, 2005). For

431   experiments, immortalized MEFs were maintained in growth medium containing high glucose

432   DMEM, 10% FBS. RAW264.7 mouse macrophages (TIB-71) and B16-F10 mouse melanoma cells

433   (CRL-6475) were purchased from ATCC. For generation of stable Bmal1 overexpressing

434   RAW264.7 cells, the *Bmal1* coding sequence was cloned from mouse embryonic cDNA (forward

435   primer: 5' GGCGAATTCGCGGACCAGAGAATGGAC 3'; reverse primer: 5'

436   GGGCTCGAGCTACAGCGGCCATGGCAA 3') and subcloned into the pBABE retroviral

437   expression vector (Addgene, 1764). Retroviral vectors were transfected into Phoenix packaging

438   cells, followed by collection of supernatants containing retroviruses. RAW264.7 macrophages

439   were incubated with retroviral supernatants with 4 µg/mL polybrene, and infected cells were

440   selected with 4 µg/mL puromycin. Control cells were transduced with the empty pBABE vector.

441

442   **Syngeneic tumor model and tumor measurement.** Male and female WT and M-BKO mice aged

443   10-12 weeks were subcutaneously injected in the right flank with 300,000 B16-F10 mouse

444   melanoma cells. For co-injection experiments, 500,000 B16-F10 cells were mixed with either

445   500,000 WT or M-BKO BMDMs (differentiation for 6 day) in the right and left flanks,

446   respectively. Tumor dimensions were measured every two days by caliper after all mice had

447   palpable tumors, and tumor volume was calculated as LxWxWx0.52 as previously

448   described(Colegio et al., 2014). For DMM treatment, mice were switched to soft pellet, high fat

449   diet (Bio-Serv, F3282) so that DMM can be mixed with the diet using a blender. The tumor growth

450   rate was slower on high fat diet (Figure 7C) compared to normal chow (Figure 7A).

451

452   **RNA sequencing.** RNA-seq was performed on RNA from 3 biological replicates per treatment.

453   Sequencing and raw data processing were conducted at the Institute of Molecular Biology (IMB)

454   Genomics Core and IMB Bioinformatics Service Core, respectively, at Academia Sinica (Taipei,

455   Taiwan, ROC). In brief, RNA was quantified using the Quant-iT ribogreen RNA reagent

456   (ThermoFisher, R11491), and RNA quality was determined using a Bioanalyzer 2100 (Agilent;

457   RIN>8, OD 260/280 and OD 260/230>1.8). RNA libraries were prepared using the TruSeq

458   Stranded mRNA Library Preparation Kit (Illumina, RS-122-2101). Sequencing was analyzed with

459   an Illumina NextSeq 500 instrument. Raw data were analyzed using the CLC Genomics

460   Workbench. Raw sequencing reads were trimmed by removing adapter sequences, low-quality

461   sequences (Phred quality score of < 20) and sequences >25 bp in length and mapped to the mouse

462   genome assembly (mm10) from University of California, Santa Cruz, using the following

463   parameters: mismatches = 2, minimum fraction length = 0.9, minimum fraction similarity = 0.9,

464   and maximum hits per read = 5. Gene expression was determined by the number of transcripts per

465   kilobase million. Functional annotation clustering of differentially regulated genes was done using

466   DAVID (https://david-d.ncifcrf.gov/), and the interaction maps of transcriptional regulators that

467   were induced or repressed by M1 activation shown in Figure 1 supplemental figure 1A were

468   generated using STRING (https://string-db.org/). Significantly changed genes were determined by

469   p<0.05 and FDR<0.05.

470

471   **qPCR.** Relative gene expression was determined by real-time qPCR with SYBR Green. The

472   expression of the ribosomal subunit *36b4* (*Rplp0*) was used as an internal control to normalize

473   expression data. Primer sequences are listed below:

474
475

Gene	Forward primer (5' to 3')	Reverse primer (5' to 3')
36b4 (Rplp0)	AGATGCAGCAGATCCGCAT	GTTCTTGCCCATCAGCACC
Arg1	CGTAGACCCTGGGGAACACTAT	TCCATCACCTTGCCAATCCC
Bckdhb	TGGGGCTCTCTACCATTCTCA	GGGGTATTACCACCTTGATCCC
Bmal1	AGGATCAAGAATGCAAGGGAGG	TGAAACTGTTCATTTTGTCCCGA
cMyc	CAGCGACTCTGAAGAAGAGCA	GACCTCTTGGCAGGGGTTTG
Cry1	CACTGGTTCCGAAAGGGACTC	CTGAAGCAAAAATCGCCACCT
Gclc	CATCCTCCAGTTCCTGCACA	ATGTACTCCACCTCGTCACC
Hif1a	GAACGAGAAGAAAAATAGGATGAGT	ACTCTTTGCTTCGCCGAGAT
Hmox1	CAGAGCCGTCTCGAGCATAG	CAAATCCTGGGGCATGCTGT
Il1b	AGCTTCAGGCAGGCAGTATC	AAGGTCCACGGGAAAGACAC
Ldha	GCGTCTCCCTGAAGTCTCTT	GCCCAGGATGTGTAACCTTT
Mgl2	CCTTGCGTTTGTCAAAACATGAC	CTGAGGCTTATGGAACTGAGGC
Mmsdh	GAGGCCTTCAGGTGGTTGAG	GATAGATGGCATGGTCTCTCCC
Nfe2l2	GGTTGCCCACATTCCCAAAC	GCAAGCGACTCATGGTCATC
Nfkb1	CCTGCTTCTGGAGGGTGATG	GCCGCTATATGCAGAGGTGT
Nqo1	TCTCTGGCCGATTCAGAGTG	TGCTGTAAACCAGTTGAGGTTC
Nr1d2	TCATGAGGATGAACAGGAACCG	CGGCCAAATCGAACAGCATC
Ppard	CAGCCTCAACATGGAATGTC	TCCGATCGCACTTCTCATAC
Pparg	CAGGAGCCTGTGAGACCAAC	ACCGCTTCTTTCAAATCTTGTCTG
Slc7a2	CCCGGGATGGCTTACTGTTT	AGGCCATCACAGCAGAAATGA
Slc7a8	GAACCACCCGGGTTCTGAC	TGATGTTCCCTACAATGATACCACA
Slc7a11	ATCTCCCCCAAGGGCATACT	GCATAGGACAGGGCTCCAAA
Stat3	TGGCAGTTCTCGTCCAC	CCAGCCATGTTTTCTTTGC

476

477

Western blot. Standard Tris-Glycine SDS-PAGEs were run and transferred to PVDF membranes

by wet transfer. Membranes were incubated with primary antibodies in TBST buffer with 1% BSA

overnight. ECL signal was imaged using a BioRad ChemiDoc XRS+ imaging system. The

antibody for Bmal1 (sc365645) was from Santa Cruz. The antibody for Hif-1α (NB100-449) was

from Novus Biologicals. The antibodies for β-tubulin (2146) and β-actin (4970) were from Cell

Signaling Technology.

Extracellular flux analyses. Extracellular flux experiments were done using a Seahorse XF24

analyzer (Agilent) and FluxPaks (Agilent, 100850-001). 200,000 BMDMs, splenic/peritoneal

23

487   macrophages or RAW264.7 cells were seeded into Seahorse XF24 plates for extracellular flux

488   experiments. Minimal DMEM (pH 7.4) without phenol red and containing energy substrates as

489   indicated was used as assay medium. 2% dialyzed FBS was added to media for experiments where

490   LPS was injected during the assay to enhance responsiveness to LPS. Assay measurements were

491   normalized to total protein content.

492

493   **Glucose uptake assay.** BMDMs were plated at a density of 1 million cells per well in 12-well

494   plates and stimulated as indicated. Cells were then washed with Krebs-Ringer bicarbonate HEPES

495   (KRBH) buffer and then given 400 µL with KRBH buffer loaded with 0.8 µCi/well [^{3}H]-2-

496   deoxyglucose (PerkinElmer, NET549A001MC) and 0.5 mM unlabeled 2-deoxyglucose and

497   incubated at 37°C for 30 minutes. 10 µL of 1.5 mM Cytochalasin B (Cayman Chemical, 11328)

498   was then added to stop glucose uptake. 400 µL of lysate was used to measure levels [^{3}H]-2-

499   deoxyglucose by a scintillation counter, and the remaining lysate was used to measure total protein

500   content for normalization.

501

502   **Measurement of lactic acid secretion.** Lactic acid was measured in the supernatants of BMDMs

503   using the Biovision Lactate Colorimetric Kit (K627) according to the manufacturer's protocol.

504   Readings were normalized to total cellular protein content.

505

506   **Mitochondrial isolation.** Mitochondria were isolated from primary BMDMs by differential

507   centrifugation. In brief, cells were resuspended in 500 µL of ice-cold mitochondrial isolation

508   buffer consisting of 70 mM sucrose, 50 mM Tris, 50 mM KCl, 10 mM EDTA, and 0.2% fatty-acid

509   free BSA (pH 7.2) and then extruded through 29-gauge syringes 20 times. Lysates were spun at

510   800g to pellet nuclei, and supernatants were spun at 8,000g to isolate mitochondria. Pelleted

511   mitochondria were washed once more with 500 μL of mitochondria isolation buffer. Total

512   mitochondrial protein content was determined by BCA assay.

513

514   **ETC activity assays in isolated mitochondria.** The activities of ETC complexes I-IV were

515   measured in isolated mitochondria using colorimetric assays as previously described (Spinazzi et

516   al., 2012) with modifications. In brief, 15 μg of mitochondria were loaded per reaction for

517   complexes III and IV, and 30 and 50 μg were used for complexes II and I, respectively. Complex

518   I activity was determined by the decrease in absorbance at 340 nm corresponding to reduction of

519   ubiquinone by electrons from NADH. Complex II activity was determined by the decrease in

520   absorbance at 600 nm corresponding to reduction of decylubiquinone by electrons from succinate.

521   Complex III activity was determined by the increase in absorbance at 550 nm corresponding to

522   reduction of cytochrome C. Complex IV activity was determined by decrease in absorbance at

523   550 nm corresponding to oxidation of cytochrome C.

524

525   **Flow cytometry.** For flow cytometry, BMDMs were seeded into low attachment plates for

526   indicated treatments and resuspended by pipetting. Mitochondrial content in BMDMs was

527   determined by flow cytometry of live cells stained with 100 μM Mitotracker Green FM

528   (ThermoFisher, M7514) according to the manufacturer's instructions.

529   For flow cytometry of tumor-infiltrating lymphocytes, cells were stimulated *ex vivo* with

530   20 ng/mL phorbol 12-myristate 13-acetate, or PMA, (Sigma-Aldrich, P8139) and 1 μg/mL

531   ionomycin (Sigma-Aldrich, I0634) for 4 hours and co-treated with brefeldin A (Cell Signaling

532   Technology, 9972) to inhibit cytokine release. Cells were stained with the fixable viability dye

533   eFluor 455uv (ThermoFisher, 65-868-14) for 20 minutes at 4°C in FACS buffer (2% FBS and 1

534   mM EDTA in PBS), washed, and incubated with antibodies against indicated surface antigens for

535   30 min at 4°C. Cells were then washed twice and fixed with 2% paraformaldehyde for 1 hour at

536   4°C and resuspended and stored in FACS buffer prior to downstream analysis. Immediately before

537   flow cytometric analysis, cells were permeabilized for intracellular staining using the

538   Foxp3/Transcription factor staining buffer set (ThermoFisher, 00-5523-00) according to the

539   manufacturer's instructions. Of viable cells, CD8$^+$ T cells were identified as CD45$^+$ CD3$^+$ CD8a$^+$

540   cells and NK cells were identified by CD45$^+$ CD3$^-$ NK1.1$^+$ staining. Antibodies for PerCp/Cy5.5-

541   conjugated CD45 (103132), PE/Cy7-conjugated CD3e (100320), Alexa Fluor 700-conjugated

542   CD8a (100730) and APC-conjugated NK1.1 (108710) were from Biolegend. The antibody for PE-

543   conjugated Ifn-γ (12-7311-81) was from ThermoFisher Scientific.

544   To measure ROS production by isolated mitochondria, 15 μg of mitochondria were

545   resuspended in 500 μL mitochondrial isolation buffer containing 5 μM MitoSox Red

546   (ThermoFisher, M36008) and 100 μM MitoTracker Green FM with or without 10 mM sodium

547   succinate. Mitochondria were incubated for 20 minutes at room temperature, washed with isolation

548   buffer, and resuspended for flow cytometry. Mitochondria were identified by side scatter and

549   positive MitoTracker Green staining for measurement of mean MitoSox Red intensity per

550   population.

551

552   **Steady-state metabolomics.** Untargeted metabolomics analysis using GC-TOF mass

553   spectrometry was conducted by the West Coast Metabolomics Center at UC Davis. In brief, 10

554   million cells were lifted, pelleted, and washed twice with PBS for each replicate. Cell lysates were

555   homogenized by metal bead beating, and metabolites were extracted using 80% methanol.

26

556 Following extraction, cell pellets were solubilized using Tris-HCl Urea buffer (pH 8.0) containing

557 1% SDS to measure cellular protein content for each sample. All metabolite readings were

558 normalized to total protein content.

559

560 **Collection of tumor-conditioned medium.** Mice bearing subcutaneous B16-F10 tumors were

561 sacrificed 20 days after injection with 500,000 cells. Tumors were dissected and weighed. Tumors

562 were minced in growth medium containing 10% dialyzed FBS in high glucose DMEM (5 mL per

563 gram of tissue) and incubated at 37°C for 2 hours. Conditioned medium was collected and filtered

564 through 100 μm strainer followed by three spins at 1,000 rpm to pellet and remove residual

565 cells/debris from the medium.

566

567 **Isolation of tumor-infiltrating immune cells.** Subcutaneous mouse tumors were dissected,

568 weighed, and then placed in 6-well plates with growth medium (RPMI, 5% FBS) and minced.

569 Minced tissues were combined into three groups per genotype, spun down in 50 mL conical tubes,

570 and resuspended in 20 mL digestion buffer (0.5 mg/mL collagenase IV, 0.1 mg/mL DNase I in

571 HBSS medium). Tumors were digested at 37°C with gentle shaking for 30 minutes and vortexed

572 every 10 minutes. Contents were filtered through a 100 mm mesh, and cells were pelleted and

573 resuspended in 45% percoll in 1X HBSS and 1X PBS. Cells were spun at 2,000 rpm at 4°C with

574 a swing bucket rotor for 20 minutes. The supernatant was aspirated, and the pellet was briefly

575 resuspended in 5 mL ACK buffer to lyse red blood cells. Lastly, cells were pelleted and

576 resuspended in growth medium for downstream applications.

577 To isolate F4/80$^+$ cells from tumors, tissues were homogenized and processed as above to

578 collect tumor-infiltrating leukocytes. F4/80$^+$ cells were then isolated by positive selection using a

27

579   rat anti-F4/80 antibody (Biolegend, 123120) and sheep anti-rat Dynabeads (ThermoFisher

580   Scientific, 11035) according to the manufacturer's instructions.

581

582   **Statistical analysis.** All data are presented as mean ± SEM. GraphPad Prism 7 was used for

583   statistical analyses. Two-tailed Student's t test was used for comparisons of two parameters. Two-

584   way ANOVA was used for multi-parameter analyses for time course comparisons. Cell-based

585   experiments were performed with 3-5 biological replicates (cell culture replicates). For tumor

586   volume, outliers were determined using a Rout test ($p < 0.05$), and outliers were omitted from

587   downstream experiments.

588

589

599

600   **AUTHOR CONTRIBUTIONS**

601   R.K.A., Y.H.L., N.H.K., K.A.S., and C.X. performed the experiments. A.L.H., S.L., and D.J.

602   generated reagents. N.S.L. assisted with RNA-seq data analysis. R.K.A. and C.H.L.

603   conceptualized the study, designed experiments, interpreted data, and wrote the manuscript.

604   C.H.L. supervised the study.

605

606   **COMPETING INTERESTS**

607   The authors declare no competing interests.

608

REFERENCES

Andrejeva, G., & Rathmell, J. C. (2017). Similarities and Distinctions of Cancer and Immune Metabolism in Inflammation and Tumors. *Cell Metab, 26*(1), 49-70. doi:10.1016/j.cmet.2017.06.004

Arts, R. J., Plantinga, T. S., Tuit, S., Ulas, T., Heinhuis, B., Tesselaar, M., . . . Netea-Maier, R. T. (2016). Transcriptional and metabolic reprogramming induce an inflammatory phenotype in non-medullary thyroid carcinoma-induced macrophages. *Oncoimmunology, 5*(12), e1229725. doi:10.1080/2162402X.2016.1229725

Bell, E. L., Klimova, T. A., Eisenbart, J., Moraes, C. T., Murphy, M. P., Budinger, G. R., & Chandel, N. S. (2007). The Qo site of the mitochondrial complex III is required for the transduction of hypoxic signaling via reactive oxygen species production. *J Cell Biol, 177*(6), 1029-1036. doi:10.1083/jcb.200609074

Buck, M. D., Sowell, R. T., Kaech, S. M., & Pearce, E. L. (2017). Metabolic Instruction of Immunity. *Cell, 169*(4), 570-586. doi:10.1016/j.cell.2017.04.004

Canaple, L., Rambaud, J., Dkhissi-Benyahya, O., Rayet, B., Tan, N. S., Michalik, L., . . . Laudet, V. (2006). Reciprocal regulation of brain and muscle Arnt-like protein 1 and peroxisome proliferator-activated receptor alpha defines a novel positive feedback loop in the rodent liver circadian clock. *Mol Endocrinol, 20*(8), 1715-1727. doi:10.1210/me.2006-0052

Chouchani, E. T., Pell, V. R., Gaude, E., Aksentijevic, D., Sundier, S. Y., Robb, E. L., . . . Murphy, M. P. (2014). Ischaemic accumulation of succinate controls reperfusion injury through mitochondrial ROS. *Nature, 515*(7527), 431-435. doi:10.1038/nature13909

Christensen, H. N., Handlogten, M. E., Lam, I., Tager, H. S., & Zand, R. (1969). A Bicyclic Amino Acid to Improve Discriminations among Transport Systems. *Journal of Biological Chemistry, 244*(6), 1510-1520.

Colegio, O. R., Chu, N. Q., Szabo, A. L., Chu, T., Rhebergen, A. M., Jairam, V., . . . Medzhitov, R. (2014). Functional polarization of tumour-associated macrophages by tumour-derived lactic acid. *Nature, 513*(7519), 559-563. doi:10.1038/nature13490

Cramer, T., Yamanishi, Y., Clausen, B. E., Förster, I., Pawlinski, R., Mackman, N., . . . Johnson, R. S. (2003). HIF-1alpha is essential for myeloid cell-mediated inflammation. *Cell, 112*(5), 645-657.

Dai, L., Bhargava, P., Stanya, K. J., Alexander, R. K., Liou, Y.-H., Jacobi, D., . . . Lee, C.-H. (2017). Macrophage alternative activation confers protection against lipotoxicity-induced cell death. *Molecular Metabolism, 6*(10), 1186-1197. doi:10.1016/j.molmet.2017.08.001

Damiola, F., Le Minh, N., Preitner, N., Kornmann, B., Fleury-Olela, F., & Schibler, U. (2000). Restricted feeding uncouples circadian oscillators in peripheral tissues from the central pacemaker in the suprachiasmatic nucleus. *Genes & development, 14*(23), 2950-2961.

654

655 Doedens, A. L., Stockmann, C., Rubinstein, M. P., Liao, D., Zhang, N., DeNardo, D. G., . . .
656   Johnson, R. S. (2010). Macrophage expression of hypoxia-inducible factor-1 alpha
657   suppresses T-cell function and promotes tumor progression. *Cancer Res, 70*(19), 7465-
658   7475. doi:10.1158/0008-5472.CAN-10-1439

659

660 Early, J. O., Menon, D., Wyse, C. A., Cervantes-Silva, M. P., Zaslona, Z., Carroll, R. G., . . .
661   Curtis, A. M. (2018). Circadian clock protein BMAL1 regulates IL-1beta in macrophages
662   via NRF2. *Proc Natl Acad Sci U S A, 115*(36), E8460-E8468.
663   doi:10.1073/pnas.1800431115

664

665 Fukuzumi, M., Shinomiya, H., Shimizu, Y., Ohishi, K., & Utsumi, S. (1996). Endotoxin-induced
666   enhancement of glucose influx into murine peritoneal macrophages via GLUT1. *Infection
667   and immunity, 64*(1), 108-112.

668

669 Ganeshan, K., & Chawla, A. (2014). Metabolic regulation of immune responses. *Annu Rev
670   Immunol, 32*, 609-634. doi:10.1146/annurev-immunol-032713-120236

671

672 Geiger, R., Rieckmann, J. C., Wolf, T., Basso, C., Feng, Y., Fuhrer, T., . . . Lanzavecchia, A.
673   (2016). L-Arginine Modulates T Cell Metabolism and Enhances Survival and Anti-tumor
674   Activity. *Cell, 167*(3), 829-842.e813. doi:10.1016/j.cell.2016.09.031

675

676 Hardin, P. E., & Panda, S. (2013). Circadian timekeeping and output mechanisms in animals.
677   *Current Opinion in Neurobiology, 23*(5), 724-731. doi:10.1016/j.conb.2013.02.018

678

679 Hotamisligil, G. S. (2017). Foundations of Immunometabolism and Implications for Metabolic
680   Health and Disease. *Immunity, 47*(3), 406-420. doi:10.1016/j.immuni.2017.08.009

681

682 Jaakkola, P., Mole, D. R., Tian, Y.-M., Wilson, M. I., Gielbert, J., Gaskell, S. J., . . . Ratcliffe, P.
683   J. (2001). Targeting of HIF-α to the von Hippel-Lindau Ubiquitylation Complex by
684   O_2-Regulated Prolyl Hydroxylation. *Science, 292*, 468-472.

685

686 Jacobi, D., Liu, S., Burkewitz, K., Kory, N., Knudsen, Nelson H., Alexander, Ryan K., . . . Lee,
687   C.-H. (2015). Hepatic Bmal1 Regulates Rhythmic Mitochondrial Dynamics and Promotes
688   Metabolic Fitness. *Cell Metabolism, 22*(4), 709-720. doi:10.1016/j.cmet.2015.08.006

689

690 Kang, K., Reilly, S. M., Karabacak, V., Gangl, M. R., Fitzgerald, K., Hatano, B., & Lee, C.-H.
691   (2008). Adipocyte-derived Th2 cytokines and myeloid PPARdelta regulate macrophage
692   polarization and insulin sensitivity. *Cell Metabolism, 7*(6), 485-495.
693   doi:10.1016/j.cmet.2008.04.002

694

695 Lamas, B., Vergnaud-Gauduchon, J., Goncalves-Mendes, N., Perche, O., Rossary, A., Vasson, M.
696   P., & Farges, M. C. (2012). Altered functions of natural killer cells in response to L-
697   Arginine availability. *Cell Immunol, 280*(2), 182-190. doi:10.1016/j.cellimm.2012.11.018

698

699   Lampropoulou, V., Sergushichev, A., Bambouskova, M., Nair, S., Vincent, Emma E.,
700   Loginicheva, E., . . . Artyomov, Maxim N. (2016). Itaconate Links Inhibition of Succinate
701   Dehydrogenase with Macrophage Metabolic Remodeling and Regulation of Inflammation.
702   *Cell Metabolism, 24*(1), 158-166. doi:10.1016/j.cmet.2016.06.004
703
704   Lee, C.-H., Kang, K., Mehl, I. R., Nofsinger, R., Alaynick, W. A., Chong, L.-W., . . . Evans, R.
705   M. (2006). Peroxisome proliferator-activated receptor δ promotes very low-density
706   lipoprotein-derived fatty acid catabolism in the macrophage. *Proceedings of the National
707   Academy of Sciences, 103*, 2434-2439.
708
709   Li, F., Wang, Y., Zeller, K. I., Potter, J. J., Wonsey, D. R., O'Donnell, K. A., . . . Dang, C. V.
710   (2005). Myc Stimulates Nuclearly Encoded Mitochondrial Genes and Mitochondrial
711   Biogenesis. *Molecular and Cellular Biology, 25*(14), 6225-6234.
712   doi:10.1128/mcb.25.14.6225-6234.2005
713
714   Liu, D., Chang, C., Lu, N., Wang, X., Lu, Q., Ren, X., . . . Tang, L. (2017). Comprehensive
715   Proteomics Analysis Reveals Metabolic Reprogramming of Tumor-Associated
716   Macrophages Stimulated by the Tumor Microenvironment. *J Proteome Res, 16*(1), 288-
717   297. doi:10.1021/acs.jproteome.6b00604
718
719   Liu, S., Brown, J. D., Stanya, K. J., Homan, E., Leidl, M., Inouye, K., . . . Lee, C.-H. (2013). A
720   diurnal serum lipid integrates hepatic lipogenesis and peripheral fatty acid use. *Nature,
721   502*(7472), 550-554. doi:10.1038/nature12710
722
723   Marpegán, L., Bekinschtein, T. A., Costas, M. A., & Golombek, D. A. (2005). Circadian responses
724   to endotoxin treatment in mice. *Journal of Neuroimmunology, 160*(1), 102-109.
725   doi:10.1016/j.jneuroim.2004.11.003
726
727   Masson, N., & Ratcliffe, P. J. (2014). Hypoxia signaling pathways in cancer metabolism: the
728   importance of co-selecting interconnected physiological pathways. *Cancer & metabolism,
729   2*(1), 3-3. doi:10.1186/2049-3002-2-3
730
731   Mills, E. L., Kelly, B., Logan, A., Costa, A. S. H., Varma, M., Bryant, C. E., . . . O'Neill, L. A.
732   (2016). Succinate Dehydrogenase Supports Metabolic Repurposing of Mitochondria to
733   Drive Inflammatory Macrophages. *Cell, 167*(2), 457-470 e413.
734   doi:10.1016/j.cell.2016.08.064
735
736   Mills, E. L., Ryan, D. G., Prag, H. A., Dikovskaya, D., Menon, D., Zaslona, Z., . . . O'Neill, L. A.
737   (2018). Itaconate is an anti-inflammatory metabolite that activates Nrf2 via alkylation of
738   KEAP1. *Nature, 556*(7699), 113-117. doi:10.1038/nature25986
739
740   Nguyen, K. D., Fentress, S. J., Qiu, Y., Yun, K., Cox, J. S., & Chawla, A. (2013). Circadian Gene
741   Bmal1 Regulates Diurnal Oscillations of Ly6C^{hi} Inflammatory Monocytes.
742   *Science, 341*, 1483-1488.
743

O'Callaghan, E. K., Anderson, S. T., Moynagh, P. N., & Coogan, A. N. (2012). Long-lasting effects of sepsis on circadian rhythms in the mouse. *PLoS One, 7*(10), e47087. doi:10.1371/journal.pone.0047087

O'Neill, L. A., Kishton, R. J., & Rathmell, J. (2016). A guide to immunometabolism for immunologists. *Nat Rev Immunol, 16*(9), 553-565. doi:10.1038/nri.2016.70

Odegaard, J. I., Ricardo-Gonzalez, R. R., Goforth, M. H., Morel, C. R., Subramanian, V., Mukundan, L., . . . Chawla, A. (2007). Macrophage-specific PPARgamma controls alternative activation and improves insulin resistance. *Nature, 447*(7148), 1116-1120. doi:10.1038/nature05894

Papagiannakopoulos, T., Bauer, Matthew R., Davidson, Shawn M., Heimann, M., Subbaraj, L., Bhutkar, A., . . . Jacks, T. (2016). Circadian Rhythm Disruption Promotes Lung Tumorigenesis. *Cell Metabolism, 24*(2), 324-331. doi:10.1016/j.cmet.2016.07.001

Peek, C. B., Affinati, A. H., Ramsey, K. M., Kuo, H. Y., Yu, W., Sena, L. A., . . . Bass, J. (2013). Circadian clock NAD+ cycle drives mitochondrial oxidative metabolism in mice. *Science, 342*(6158), 1243417. doi:10.1126/science.1243417

Penny, H. L., Sieow, J. L., Adriani, G., Yeap, W. H., See Chi Ee, P., San Luis, B., . . . Wong, S. C. (2016). Warburg metabolism in tumor-conditioned macrophages promotes metastasis in human pancreatic ductal adenocarcinoma. *Oncoimmunology, 5*(8), e1191731. doi:10.1080/2162402X.2016.1191731

Robb, E. L., Hall, A. R., Prime, T. A., Eaton, S., Szibor, M., Viscomi, C., . . . Murphy, M. P. (2018). Control of mitochondrial superoxide production by reverse electron transport at complex I. *J Biol Chem, 293*(25), 9869-9879. doi:10.1074/jbc.RA118.003647

Rodriguez-Prados, J. C., Traves, P. G., Cuenca, J., Rico, D., Aragones, J., Martin-Sanz, P., . . . Bosca, L. (2010). Substrate fate in activated macrophages: a comparison between innate, classic, and alternative activation. *J Immunol, 185*(1), 605-614. doi:10.4049/jimmunol.0901698

Segawa, H., Fukasawa, Y., Miyamoto, K.-i., Takeda, E., Endou, H., & Kanai, Y. (1999). Identification and Functional Characterization of a Na+-independent Neutral Amino Acid Transporter with Broad Substrate Selectivity. *Journal of Biological Chemistry, 274*(28), 19745-19751.

Semenza, G. L., Roth, P. H., Fang, H. M., & Wang, G. L. (1994). Transcriptional regulation of genes encoding glycolytic enzymes by hypoxia-inducible factor 1. *Journal of Biological Chemistry, 269*(38), 23757-23763.

Sinclair, L. V., Rolf, J., Emslie, E., Shi, Y. B., Taylor, P. M., & Cantrell, D. A. (2013). Control of amino-acid transport by antigen receptors coordinates the metabolic reprogramming essential for T cell differentiation. *Nat Immunol, 14*(5), 500-508. doi:10.1038/ni.2556

790

791 Spinazzi, M., Casarin, A., Pertegato, V., Salviati, L., & Angelini, C. (2012). Assessment of
792   mitochondrial respiratory chain enzymatic activities on tissues and cultured cells. *Nat
793   Protoc, 7*(6), 1235-1246. doi:10.1038/nprot.2012.058
794

795 Steggerda, S. M., Bennett, M. K., Chen, J., Emberley, E., Huang, T., Janes, J. R., . . . Gross, M. I.
796   (2017). Inhibition of arginase by CB-1158 blocks myeloid cell-mediated immune
797   suppression in the tumor microenvironment. *J Immunother Cancer, 5*(1), 101.
798   doi:10.1186/s40425-017-0308-4
799

800 Tamaru, T., Isojima, Y., van der Horst, G. T. J., Takei, K., Nagai, K., & Takamatsu, K. (2003).
801   Nucleocytoplasmic shuttling and phosphorylation of BMAL1 are regulated by circadian
802   clock in cultured fibroblasts. *Genes to Cells, 8*(12), 973-983. doi:10.1046/j.1365-
803   2443.2003.00686.x
804

805 Tannahill, G. M., Curtis, A. M., Adamik, J., Palsson-McDermott, E. M., McGettrick, A. F., Goel,
806   G., . . . O'Neill, L. A. (2013). Succinate is an inflammatory signal that induces IL-1beta
807   through HIF-1alpha. *Nature, 496*(7444), 238-242. doi:10.1038/nature11986
808

809 Tsukishiro, T., Shimizu, Y., Higuchi, K., & Watanabe, A. (2000). Effect of branched-chain amino
810   acids on the composition and cytolytic activity of liver-associated lymphocytes in rats.
811   *Journal of Gastroenterology and Hepatology, 15*(8), 849-859. doi:10.1046/j.1440-
812   1746.2000.02220.x
813

814 West, A. P., Brodsky, I. E., Rahner, C., Woo, D. K., Erdjument-Bromage, H., Tempst, P., . . .
815   Ghosh, S. (2011). TLR signalling augments macrophage bactericidal activity through
816   mitochondrial ROS. *Nature, 472*(7344), 476-480. doi:10.1038/nature09973
817

818 Xu, J. (2005). Preparation, Culture, and Immortalization of Mouse Embryonic Fibroblasts. *Current
819   Protocols in Molecular Biology, 70*(1), 28.21.21-28.21.28.
820   doi:doi:10.1002/0471142727.mb2801s70
821

822 Yang, X., Downes, M., Yu, R. T., Bookout, A. L., He, W., Straume, M., . . . Evans, R. M. (2006).
823   Nuclear receptor expression links the circadian clock to metabolism. *Cell, 126*(4), 801-810.
824   doi:10.1016/j.cell.2006.06.050
825

826 Zhang, H., Bosch-Marce, M., Shimoda, L. A., Tan, Y. S., Baek, J. H., Wesley, J. B., . . . Semenza,
827   G. L. (2008). Mitochondrial Autophagy Is an HIF-1-dependent Adaptive Metabolic
828   Response to Hypoxia. *Journal of Biological Chemistry, 283*(16), 10892-10903.
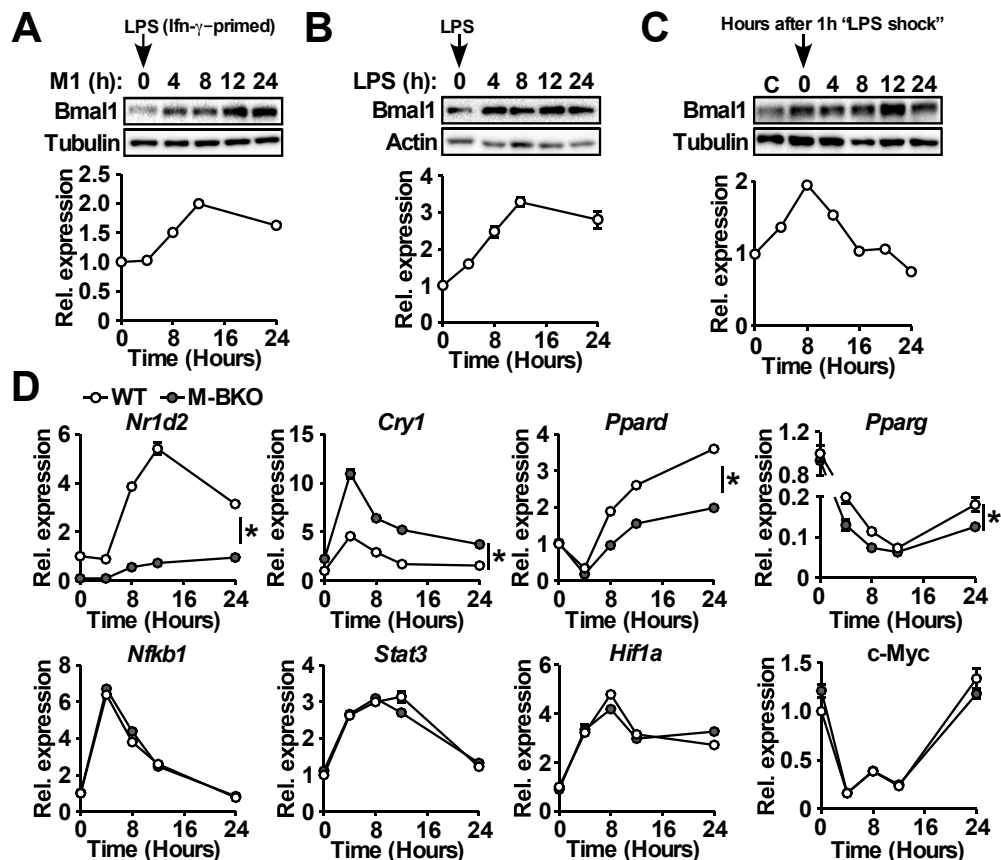829   doi:10.1074/jbc.M800102200
830

831

FIGURES

Figure 1. Macrophage Bmal1 is induced by M1 activation.
(**A**), (**B**), and (**C**) Bmal1 protein levels (top) and relative gene expression determined by qPCR (bottom) in bone marrow-derived macrophages during a 24-hour time course of M1 activation (10 ng/ml Ifn-γ overnight priming + 10 ng/ml LPS) (A), treatment with LPS alone (100 ng/ml) (B), or acute LPS treatment for 1 hour (100 ng/mL) (C). For M1 and LPS only treatments, LPS was spiked in at time zero without medium change. For acute LPS treatment, cells were given with LPS for one hour followed by culture in DMEM, 2% FBS without LPS (time zero indicates medium change). N=3 biological replicates for qPCR. (**D**) Relative expression of circadian clock and inflammatory transcriptional regulators in M1-activated macrophages determined by qPCR. N=3 biological replicates, statistical analysis performed using 2-way ANOVA for WT vs. M-BKO across the time course. Data presented as mean ± S.E.M. *p<0.05. Experiments were repeated at least twice.
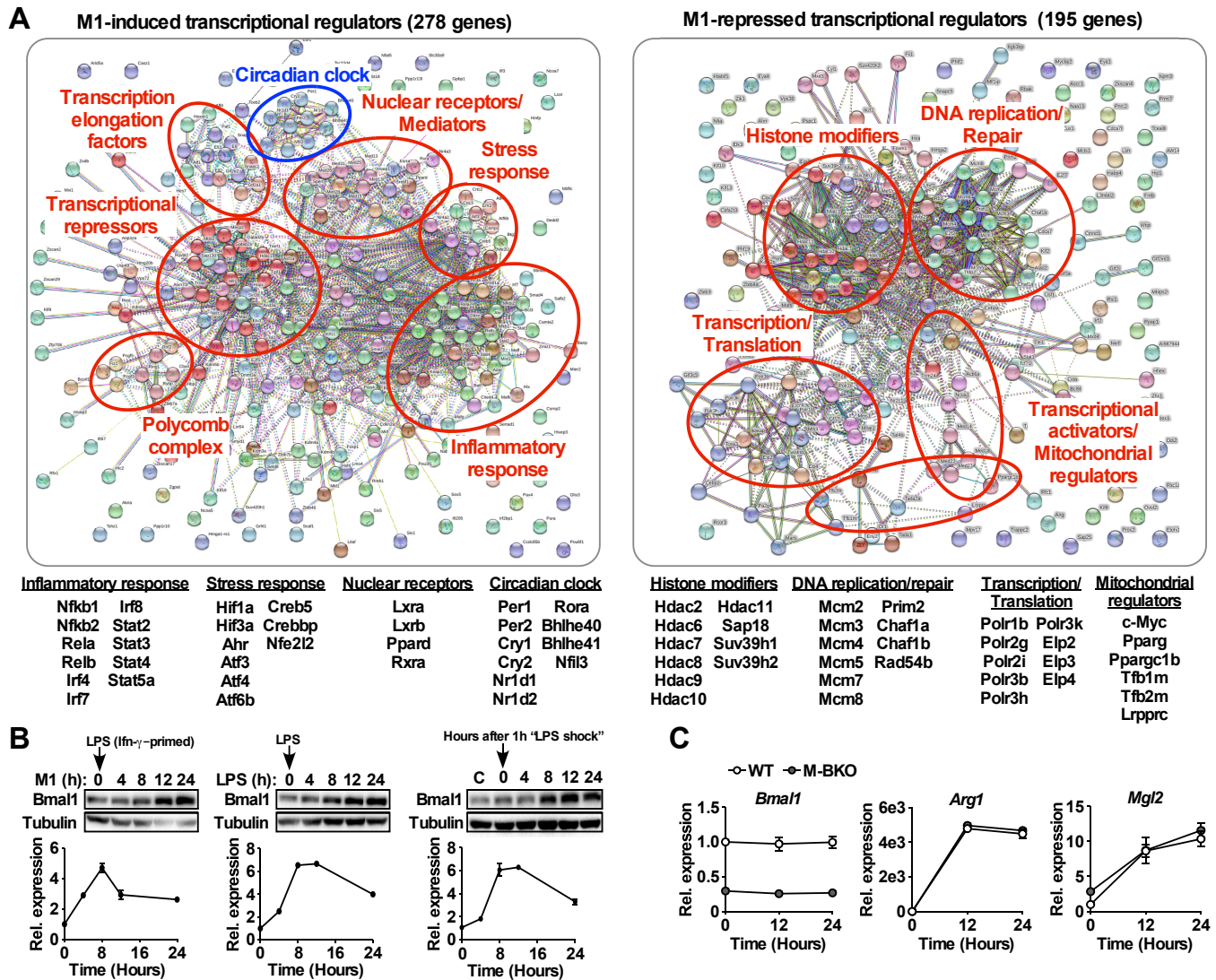
A

M1-induced transcriptional regulators (278 genes)

M1-repressed transcriptional regulators (195 genes)

Left map labels: Transcription elongation factors; Circadian clock; Nuclear receptors/Mediators; Stress response; Transcriptional repressors; Polycomb complex; Inflammatory response

Right map labels: Histone modifiers; DNA replication/Repair; Transcription/Translation; Transcriptional activators/Mitochondrial regulators

Inflammatory response		Stress response		Nuclear receptors		Circadian clock	
Nfkb1	Irf8	Hif1a	Creb5	Lxra		Per1	Rora
Nfkb2	Stat2	Hif3a	Crebbp	Lxrb		Per2	Bhlhe40
Rela	Stat3	Ahr	Nfe2l2	Ppard		Cry1	Bhlhe41
Relb	Stat4	Atf3		Rxra		Cry2	Nfil3
Irf4	Stat5a	Atf4				Nr1d1	
Irf7		Atf6b				Nr1d2	

Histone modifiers		DNA replication/repair		Transcription/Translation		Mitochondrial regulators	
Hdac2	Hdac11	Mcm2	Prim2	Polr1b	Polr3k	c-Myc	
Hdac6	Sap18	Mcm3	Chaf1a	Polr2g	Elp2	Pparg	
Hdac7	Suv39h1	Mcm4	Chaf1b	Polr2i	Elp3	Ppargc1b	
Hdac8	Suv39h2	Mcm5	Rad54b	Polr3b	Elp4	Tfb1m	
Hdac9		Mcm7		Polr3h		Tfb2m	
Hdac10		Mcm8				Lrpprc	

B

LPS (Ifn-γ−primed)
M1 (h): 0 4 8 12 24
Bmal1
Tubulin
Rel. expression (0–6) vs Time (Hours) 0 8 16 24

LPS
LPS (h): 0 4 8 12 24
Bmal1
Tubulin
Rel. expression (0–8) vs Time (Hours) 0 8 16 24

Hours after 1h "LPS shock"
C 0 4 8 12 24
Bmal1
Tubulin
Rel. expression (0–8) vs Time (Hours) 0 8 16 24

C

○ WT   ● M-BKO

Bmal1 — Rel. expression (0–1.5) vs Time (Hours) 0 12 24
Arg1 — Rel. expression (0–6e3) vs Time (Hours) 0 12 24
Mgl2 — Rel. expression (0–15) vs Time (Hours) 0 12 24

Figure 1 supplemental figure 1. The circadian clock is a transcriptional module induced by M1 activation.

(**A**) Annotated protein-protein interaction maps generated by STRING of transcriptional regulators that were significantly induced (left) or repressed (right) in WT macrophages by 8 hours M1 activation (Ifn-γ priming followed by stimulation with 10 ng/mL LPS) compared to time-matched controls (Ifn-γ priming without LPS), determined by RNA-seq ($p<0.05$, FDR<0.05, |F.C.|>1.5). N=3 biological replicates. F.C.: fold change. See Supplemental table 1 for the complete gene list. (**B**) Bmal1 protein levels (top panels) and relative gene expression determined by qPCR (bottom panels) in mouse embryonic fibroblasts during a 24 hour time course of M1 activation (10 ng/ml Ifn-γ overnight priming + 10 ng/ml LPS, left panels), treatment with LPS only (100 ng/ml, middle panels), or 1-hour acute LPS treatment (100 ng/mL, right panels). For M1 and LPS only treatment, LPS was spiked in at time zero without medium change. For acute LPS treatment, cells were given with LPS for one hour followed by culture in DMEM, 2% FBS without LPS (time zero indicates medium change). N=3 biological replicates for qPCR. (**C**) Gene expression during a 24-hour time course of Il-4 treatment in WT and M-BKO macrophages determined by qPCR. N=3 biological replicates. Data presented as mean ± S.E.M. *$p<0.05$. Cell culture experiments were repeated at least twice.

Figure 1 supplemental table 1. Transcriptional regulators differentially regulated in M1 activated macrophages.

Genes encoding transcriptional regulators that were significantly induced or repressed by 8h M1 stimulation (p<0.05, FDR<0.05, |F.C.|>1.5) in WT bone marrow derived macrophages were identified by gene ontology analysis using the DAVID platform. Differentially regulated genes that matched the Transcription GO term in the Biological Processes GO database (accession GO:0006350) were used to generate a protein-protein interaction map using String (Supplemental figure 1). Uncharacterized zinc finger proteins (ZFPs) were omitted from analyses by String. Genes are listed below:

Induced (278 genes)

ADAR	CRY1	GTF2A1	KDM4B	MNT	PPP1R10	SNAPC1	ZKSCAN17
AFF1	CRY2	GTF2E2	KDM5B	MXD1	PPP1R13L	SNAPC2	ZMIZ1
AFF4	CSRNP1	GTF2F1	KDM5C	MXI1	PTOV1	SOX5	ZSCAN2
AHR	CSRNP2	HBP1	KEAP1	MYB	PTRF	SPEN	ZSCAN29
AKNA	DAXX	HDAC1	KLF11	NAB2	PURA	SPIC	ZXDB
ANP32A	DDIT3	HES1	KLF16	NACC1	RBPJ	SREBF1	
ARHGAP22	DDX54	HES7	KLF4	NCOA5	RCOR2	SRF	
ARID3A	DEDD2	HEXIM1	KLF7	NCOA7	REL	ST18	
ARID5A	DNMT3A	HIC1	KLF9	NCOR2	RELA	STAT2	
ARNT2	DPF1	HIC2	LCOR	NFAT5	RELB	STAT3	
ASF1A	DRAP1	HIF1A	LCORL	NFE2L2	REST	STAT4	
ATF3	E2F5	HIF3A	LHX2	NFIL3	RFX1	STAT5A	
ATF4	E4F1	HINFP	LIN54	NFKB1	RING1	TAF1C	
ATF6B	EAF1	HIVEP1	LITAF	NFKB2	RNF2	TAF7	
ATXN7L3	EDF1	HIVEP2	LMO4	NFKBIZ	RORA	TAL1	
BANP	EGR2	HIVEP3	MAF	NOTCH1	RREB1	TBL1X	
BATF	EID3	HLX	MAFF	NPTXR	RSLCAN18	TCEB2	
BCL3	EIF2C1	HMG20B	MAFG	NR1D1	RUNX2	TCF4	
BCL6	ELK1	HMGA1	MAFK	NR1D2	RUNX3	TGIF1	
BCORL1	ELL	HMGA1-RS1	MAML1	NR1H2	RUVBL2	THAP7	
BHLHE40	ELL2	HMGN5	MAX	NR1H3	RXRA	TLE2	
BHLHE41	ELL3	HOPX	MBD2	NR2F6	RYBP	TLE3	
BRWD1	EPAS1	HSF4	MDFIC	NR4A1	SAFB2	TRERF1	
BTG2	ERF	IFI205	MECP2	NR4A2	SAP130	TRIB3	
CAMTA2	ERN1	IFT57	MED13	NR4A3	SAP30	TRRAP	
CASZ1	ESRRA	ILF3	MED13L	PAF1	SBNO2	TSC22D4	
CBX4	ETS1	ING2	MED15	PAX4	SCAF1	TSHZ1	
CCDC85B	ETV3	IRF2BP1	MED25	PCGF3	SEC14L2	USP49	
CDKN2A	FIZ1	IRF4	MED26	PCGF5	SERTAD1	VPS72	
CEBPB	FLII	IRF7	MED28	PER1	SETD8	WHSC1L1	
CEBPD	FOXP1	IRF8	MED31	PER2	SFPI1	ZBTB17	
CITED4	FOXP4	JARID2	MEF2D	PHF1	SIN3B	ZBTB24	
CREB5	GATA2	JDP2	MIER2	PHF12	SIX1	ZBTB46	
CREBBP	GATAD2A	JMJD6	MIER3	PIAS4	SIX5	ZBTB7A	
CREBL2	GATAD2B	JUN	MITF	PML	SLC30A9	ZBTB7B	
CREBZF	GFI1	JUNB	MIXL1	POU2F2	SMAD3	ZEB1	
CREM	GLIS3	JUND	MKL1	POU3F1	SMAD4	ZFHX4	
CRTC2	GPBP1	KDM3A	MLL1	POU6F1	SMAD7	ZGPAT	
CRTC3	GRHL1	KDM4A	MNDA	PPARD	SMYD1	ZHX2	

Repressed (195 genes)

ACTL6A	ELK3	IRF2	NAA15	SAP18
AHRR	ELP2	ITGB3BP	NCOA1	SAP25
AI987944	ELP3	KDM2B	NCOA3	SETD7
ANG	ELP4	KLF10	NFATC1	SETDB1
ASCC1	ENY2	KLF13	NFATC2	SNAPC5
ASF1B	ERCC8	KLF2	NFIA	SP3
ATAD2	ESR1	KLF8	NKRF	SSBP2
AW146154	ETOHI1	L3MBTL2	NPAT	SSRP1
BCL9L	ETV1	LBH	NPM3	STAT1
CBFA2T3	EYA1	LRPPRC	NR2C1	SUV39H1
CBX3	EYA4	LYL1	NRIP1	SUV39H2
CBX6	EZH2	MAFB	OVOL2	SUV420H2
CBX8	FLI1	MARS	PA2G4	TADA1
CCNH	FNTB	MBTPS2	PHF19	TADA2A
CDCA7	FOXM1	MCM2	PHTF2	TAF4B
CDCA7L	GTF2H2	MCM3	PNRC2	TAF9B
CEBPA	GTF2I	MCM4	POLR1B	TBX6
CEBPG	GTF2IRD1	MCM5	POLR2G	TCEA3
CEBPZ	GTF3A	MCM6	POLR2I	TCEAL8
CHAF1A	GTF3C5	MCM7	POLR3B	TCF7L2
CHAF1B	HABP4	MCM8	POLR3H	TFB1M
CHD9	HDAC10	MCTS1	POLR3K	TFB2M
CHURC1	HDAC11	MED14	PPARG	TFDP2
CIITA	HDAC2	MED18	PPARGC1B	THOC1
CIR1	HDAC6	MED22	PRIM1	TLE1
CREB3	HDAC7	MED27	PRIM2	TRAPPC2
CREB3L1	HDAC8	MEF2A	PRMT7	TRIM24
CREB3L2	HDAC9	MEF2C	PROX2	TWISTNB
CTNND1	HELLS	MEIS1	PSPC1	TXNIP
CUX1	HHEX	MLF1IP	RAD54B	UHRF1
DDI2	HIP1	MLL3	RB1	USF1
DNMT1	HIRA	MLLT3	RBAK	VGLL4
DR1	HMBOX1	MNAT1	RCBTB1	VPS36
E2F1	HMGA2	MPV17	RCOR3	WTIP
E2F2	HOXA1	MXD3	RERE	ZBTB3
E2F6	HTATSF1	MXD4	RFC1	ZBTB8A
E2F7	IKBKAP	MYBL2	RPAP1	ZHX1
E2F8	IKZF2	MYC	RSC1A1	ZIK1
EGR3	IL16	MYCBP2	RSL1	ZKSCAN4
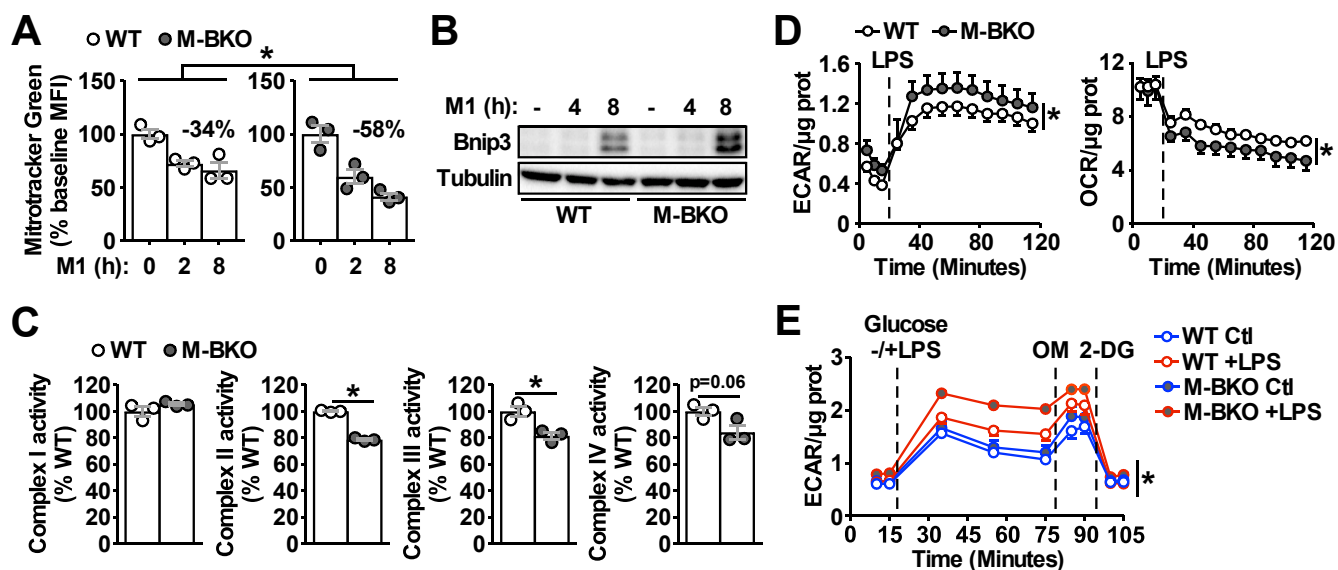
Figure 2. Bmal1 is required to maintain mitochondrial metabolism.
(**A**) Assessment of mitochondrial mass in macrophages throughout a time course of M1 activation using Mitotracker Green (mean fluorescence intensity, MFI) determined by flow cytometry. N=3 biological replicates, statistical analysis performed using 2-way ANOVA for WT vs. M-BKO across the time course. (**B**) Immunoblot of the mitophagy regulator Bnip3 in M1-activated WT and M-BKO BMDMs. (**C**) Activities of ETC complexes in isolated mitochondria from WT and M-BKO macrophages after 6 hours M1 stimulation. N=3 biological replicates, statistical analysis performed using Student's T test. (**D**) Extracellular flux analysis in Ifn-γ-primed macrophages measuring the changes in extracellular acidification rate (ECAR, left panel) and oxygen consumption rate (OCR, right panel) following LPS injection (100 ng/mL). Assay medium contained 5 mM glucose and 1 mM pyruvate in minimal DMEM with 2% dialyzed FBS, pH 7.4. N=5 biological replicates, statistical analysis performed using 2-way ANOVA for WT vs. M-BKO across the time course. (**E**) Glycolytic stress test in Ifn-γ-primed macrophages measuring ECAR following glucose (25 mM) injection, with or without LPS (100 ng/mL). Maximal glycolytic rate was determined by injection of oligomycin (OM, 2 μM), and glycolysis-dependent ECAR was determined by injection with 2-deoxyglucose (2-DG, 50 mM). Assay medium contained minimal DMEM with 2% dialyzed FBS, pH 7.4. N=5 biological replicates, statistical analysis performed using 2-way ANOVA for WT vs. M-BKO across the time course. Data presented as mean ± S.E.M. *$p < 0.05$. Experiments were repeated at least twice.
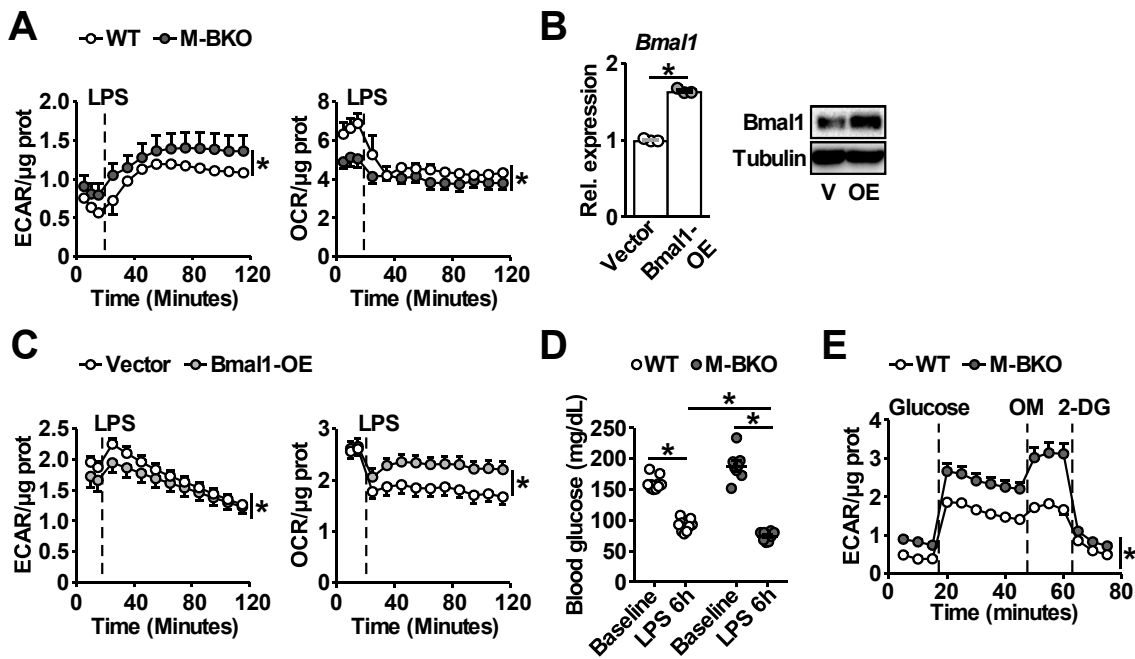
Figure 2 supplemental figure 1. Effects of *Bmal1* gene deletion and over-expression on glycolytic versus oxidative metabolism.

(**A**) Extracellular flux analysis of thioglycollate-elicited peritoneal macrophages measuring the changes in ECAR (left panel) and OCR (right panel) following LPS injection (final conc. 1 μg/mL). Assay medium contained 5 mM glucose and 1 mM pyruvate in minimal DMEM with 2% dialyzed FBS, pH 7.4. N=5 biological replicates, statistical analysis performed using 2-way ANOVA for WT vs. M-BKO across the time course. (**B**) *Bmal1* mRNA expression determined by qPCR (left) and protein levels (right) in RAW264.7 macrophage stable lines. Bmal1 OE: Bmal1 over-expressing stable line. Cells transduced with empty vector were used as the control. N=3 biological replicates for qPCR, statistical analysis performed using Student's T test. V: vector control; OE: Bmal1 over-expression. (**C**) Measurement of the changes in ECAR (left) and OCR (right) in Ifn-γ-primed RAW264.7 stable lines after injection with LPS (final conc. 100 ng/mL). Assay medium contained 25 mM glucose and 1 mM pyruvate in minimal DMEM with 2% dialyzed FBS, pH 7.4. N=5 biological replicates, statistical analysis performed using 2-way ANOVA for control vs. Bmal1 OE across the time course. (**D**) Blood glucose levels in 4-month-old WT and M-BKO male mice before and 6 h after i.p. injection with 10 μg LPS per g body weight. N=10 mice, statistical analysis performed using Student's T test. (**E**) Glycolytic stress test in splenic macrophages isolated from mice in (D) that were sacrificed 6 h after LPS injection. ECAR was measured before and after injection with glucose (25 mM). Maximal glycolytic rate was determined by injection of oligomycin (OM, 2 μM). Glycolysis-dependent ECAR was determined by injection with 2-deoxyglucose (2-DG, 50 mM). Assay medium contained minimal DMEM, pH 7.4. N=10 biological replicates, statistical analysis performed using 2-way ANOVA for WT vs. M-BKO across the time course. Data presented as mean ± S.E.M. *$p < 0.05$. Experiments were repeated at least twice.
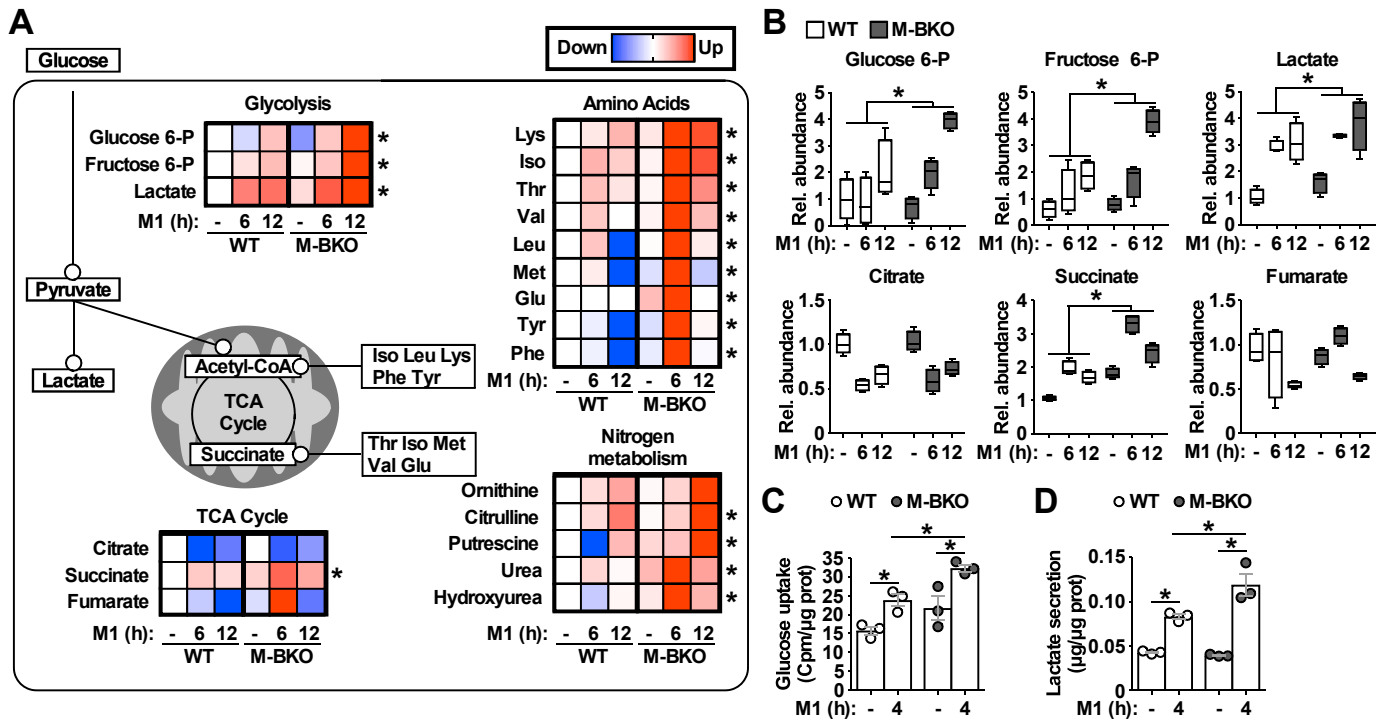
Figure 3. *Bmal1* deletion induces a metabolic shift for glycolytic and amino acid metabolism.
(**A**) Summary of steady-state metabolomics data for differentially regulated metabolites from WT and M-BKO macrophages throughout a 12-hour M1 activation time course. Data presented as heat maps (normalized to WT control for each metabolite, each panel is the average of 4 biological replicates). Statistical analysis performed using 2-way ANOVA for WT vs. M-BKO across the time course. (**B**) Box plots of relative abundances for select metabolites in (A). (**C**) and (**D**) Uptake of [³H]-2-deoxyglucose and lactate secretion in control or M1-activated macrophages. N=3 biological replicates, statistical analysis performed using Student's T test. Cell culture assays were repeated at least twice.
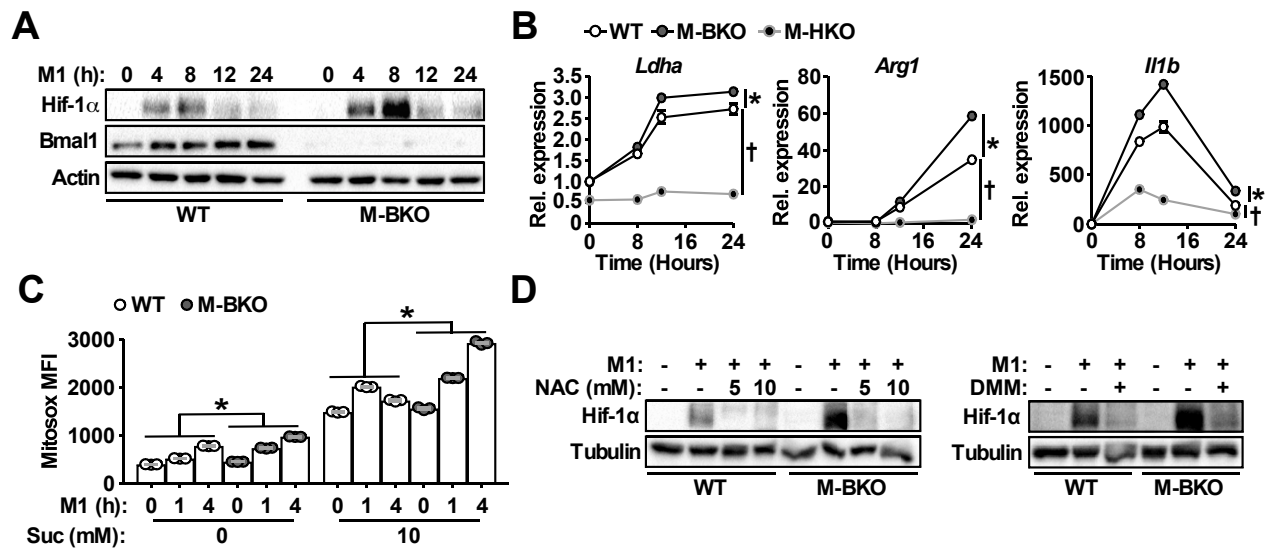
Figure 4. *Bmal1* loss-of-function increases oxidative stress and Hif-1α protein accumulation.
(**A**) Immunoblots of Hif-1α and Bmal1 protein levels in WT and M-BKO macrophages during a 24-hour time course of M1 activation. (**B**) Relative expression of Hif-1α target genes in WT, M-BKO and M-HKO macrophages determined by qPCR. N=3 biological replicates, statistical analysis performed using 2-way ANOVA for WT vs. M-BKO or WT vs. M-HKO across the time course. (**C**) Measurement of mROS using MitoSox Red (mean fluorescence intensity, MFI) in mitochondria isolated from control or M1-activated macrophages. Succinate (Suc, 10 mM) was included during MitoSox Red staining where indicated. N=3 biological replicates, statistical analysis was performed using 2-way ANOVA for WT vs. M-BKO across the time course. (**D**) Hif-1α protein levels in control or 8 hours M1-activated macrophages co-treated with or without N-acetylcysteine (NAC) or 10 mM dimethylmalonate (DMM). Data presented as mean ± S.E.M. *p<0.05 for WT vs. M-BKO and †p<0.05 for WT vs. M-HKO. Experiments were repeated at least twice.
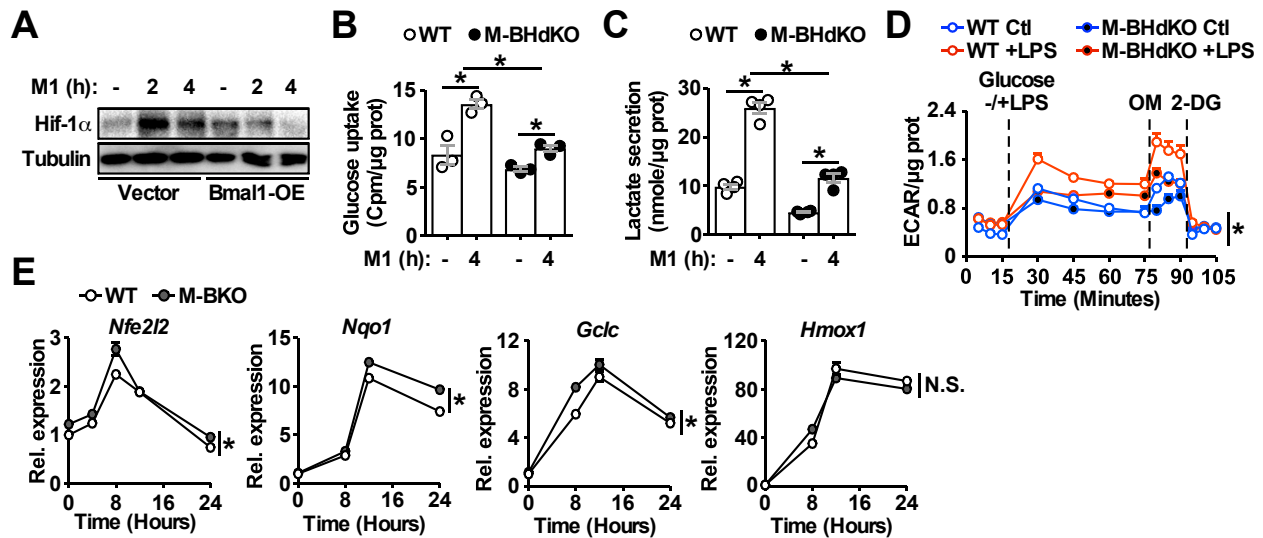
Figure 4 supplemental figure 1. Increased oxidative stress and Hif-1α activity in M1 activated M-BKO macrophages.

(**A**) Hif-1α protein levels in M1-activated (primed with 10 ng/mL Ifn-γ and stimulated with 50 ng/mL LPS) control and Bmal1 OE RAW264.7 stable lines. (**B**) and (**C**) Uptake of [³H]-2-deoxyglucose and lactate secretion in control or M1-activated macrophages. N=3 biological replicates, statistical analysis performed using Student's T test. M-BHdko: myeloid-specific *Bmal1* and *Hif1a* double knockout. (**D**) Glycolytic stress test in Ifn-γ-primed macrophages measuring ECAR following glucose (25 mM) injection without or with LPS (100 ng/mL). Maximal glycolytic rate was determined by injection of oligomycin (OM, 2 μM), and glycolysis-dependent ECAR was determined by injection with 2-deoxyglucose (2-DG, 50 mM). Assay medium contained minimal DMEM with 2% dialyzed FBS, pH 7.4. N=5 biological replicates. The difference between LPS-treated WT and M-BHdKO macrophages was determined by 2-way ANOVA across the time course. (**E**) Expression of Nrf2 target genes determined by qPCR throughout a 24-hour time course following M1 stimulation. N=3 biological replicates, statistical analysis using 2-way ANOVA for WT vs. M-BKO across the time course. Data presented as mean ± S.E.M. *p<0.05. Experiments were repeated at least twice.
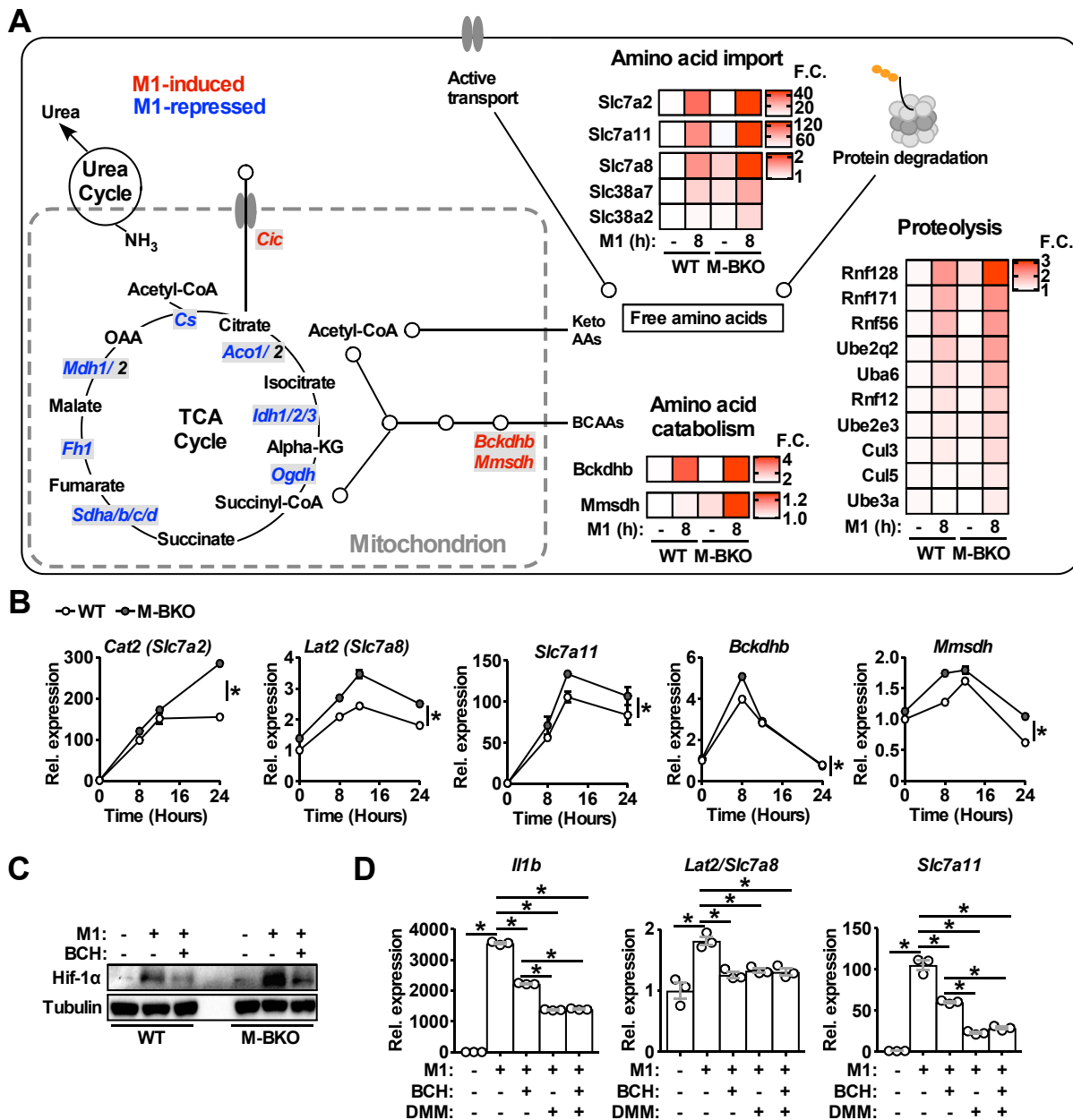
Figure 5. Genes involved in amino acid uptake and catabolism are up-regulated in M-BKO macrophages.
(**A**) Schematic representation of M1-regulated genes involved in amino acid and TCA metabolism determined by RNA-seq. Genes in blue are downregulated while genes in red are upregulated by 8 hours M1 activation in both WT and M-BKO macrophages. Genes differentially regulated between genotypes are displayed in heat maps on the right. F.C: fold change. N=3 biological replicates. BCAAs: branch chain amino acids; Keto AAs: ketogenic amino acids; Cic: mitochondrial citrate carrier. (**B**) Relative expression of differentially regulated genes identified by RNA-seq and validated by qPCR in a 24-hour time course of M1 activation. N=3 biological replicates, statistical analysis performed using 2-way ANOVA for WT vs. M-BKO across the time course. (**C**) Hif-1α protein levels in control or 6 hours M1-activated macrophages with or without co-treatment of the neutral amino acid transport inhibitor 2-amino-2-norbornanecarboxylic acid (BCH, 10 mM). (**D**) Gene expression in control or 6 hours M1-activated macrophages with or without co-treatment of 10 mM BCH and/or the complex II inhibitor dimethyl malonate (DMM, 10 mM) determined by qPCR. N=3 biological replicates, statistical analysis performed using Student's T test. Data presented as mean ± S.E.M. *p<0.05. Cell culture experiments were repeated at least twice.
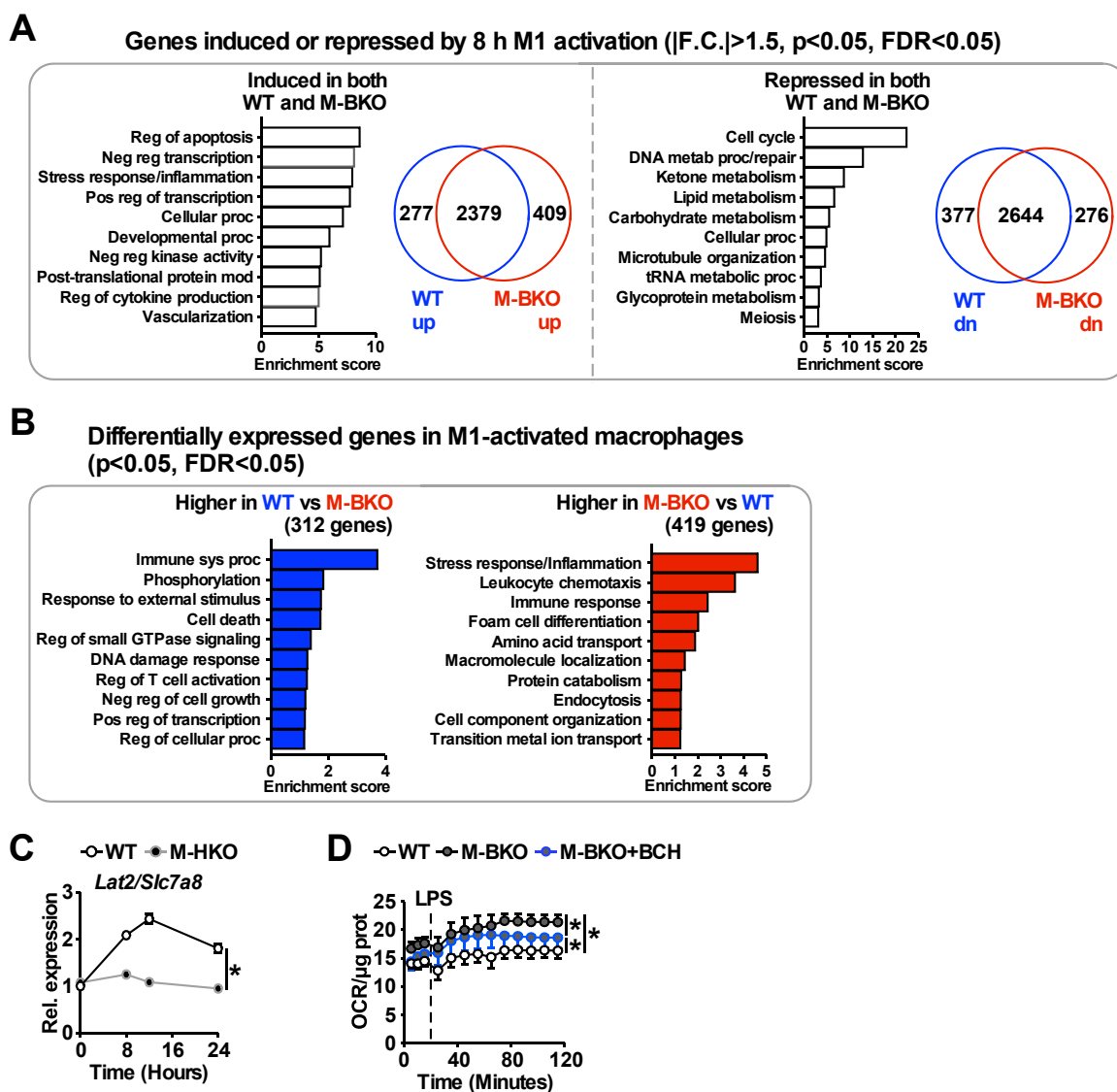
Figure 5 supplemental figure 1. Transcriptome analysis of genes regulated by M1 stimulation in WT and M-BKO macrophages.

(**A**) Functional annotation clustering by biological process and venn diagram of genes identified by RNA-seq that are mutually induced (2,379 genes, left) or suppressed (2,644 genes, right) by 8 h M1 activation in WT and M-BKO macrophages. N=3 biological replicates. F.C.: fold change. (**B**) Enriched biological processes in direct comparison of differentially expressed genes between M1-activated WT and M-BKO macrophages. (**C**) Relative expression of the neutral amino acid transporter *Slc7a8* (*Lat2*) in WT and myeloid *Hif1a* knockout (M-HKO) macrophages determined by qPCR. WT samples were from Figure 5B. N=3 biological replicates, statistical analysis performed using 2-way ANOVA for WT vs. M-HKO across the time course. (**D**) Determination of glutamine utilization by extracellular flux analysis. OCR was measured before and after LPS injection (final conc. 1 µg/mL), and assay medium contained 5 mM glutamine in minimal DMEM with 2% dialyzed FBS, pH 7.4. N=5 biological replicates, statistical analysis performed using 2-way ANOVA for WT vs. M-BKO and WT or M-BKO vs M-BKO cells co-treated with the neutral amino acid transport inhibitor 2-amino-2-norbornanecarboxylic acid (BCH, 10 mM) across the time course. Data presented as mean ± S.E.M. *p<0.05. Experiments were repeated at least twice.
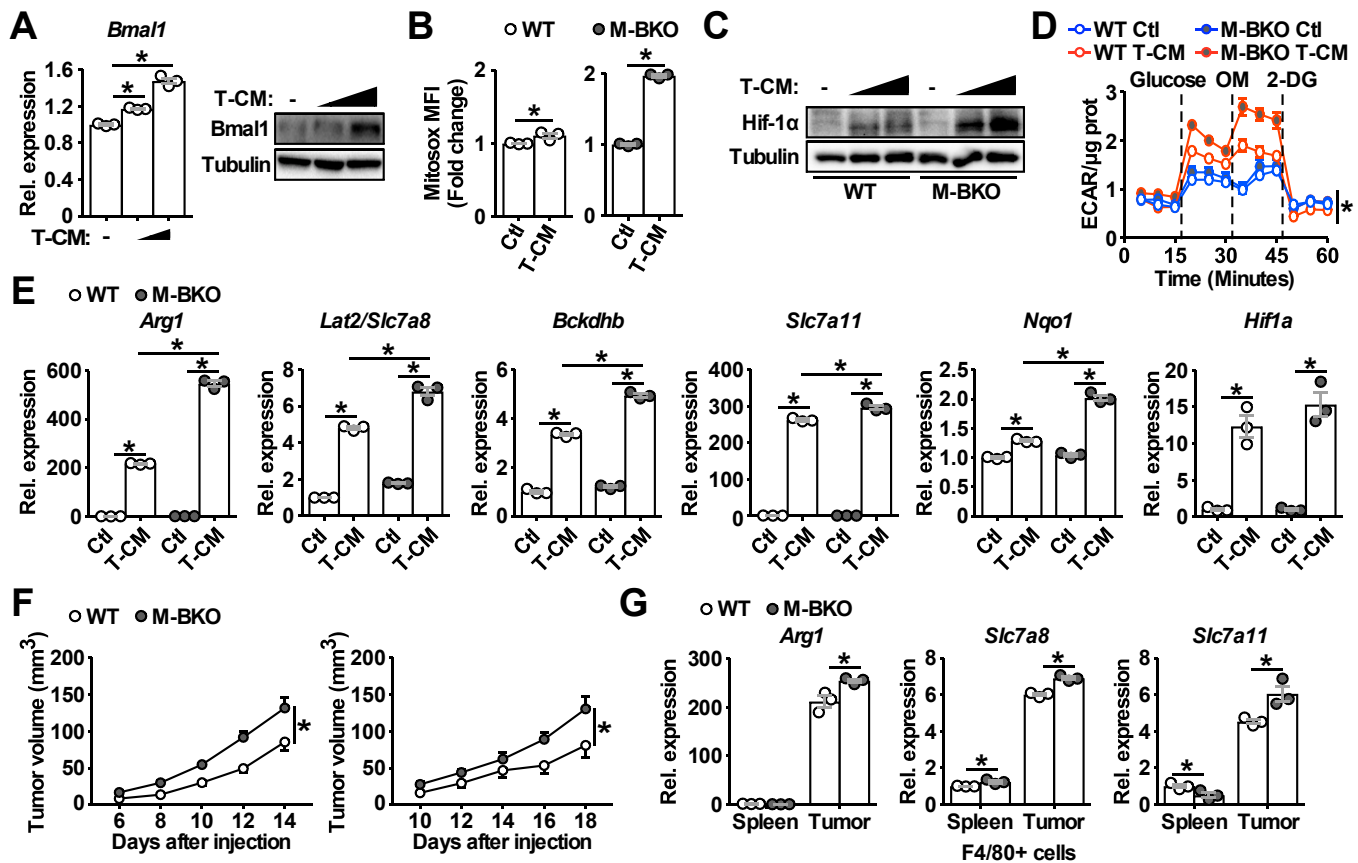
Figure 6. Bmal1 regulates tumor-associated macrophage polarization.
(**A**) Bmal1 gene expression (left panel) and protein levels (right panel) in WT macrophages treated with control medium or increasing doses of B16-F10 tumor-conditioned medium (T-CM, diluted 1:3 or 1:1 with control medium) for 8 hours. N=3 biological replicates for qPCR, statistical analysis performed using Student's T test. (**B**) Measurement of mROS using MitoSox Red (mean fluorescent intensity, MFI) in mitochondria from macrophages treated with control medium or T-CM diluted 1:1 with control medium for 1 hour. N=3 biological replicates, statistical analysis performed using Student's T test. (**C**) Hif-1α protein levels in WT and M-BKO macrophages treated with control medium, T-CM diluted 1:1 with control medium, or undiluted T-CM for 4 hours. (**D**) Glycolytic stress test in macrophages pretreated with control medium or T-CM diluted 1:1 with control medium for 4 hours. . N=5 biological replicates. Statistical analysis performed using 2-way ANOVA comparing T-CM-treated M-BKO vs. WT cells across the time course. (**E**) Relative expression of genes involved in amino acid metabolism and oxidative stress response in macrophages treated with control medium or T-CM diluted 1:3 with control medium for 8 hours determined by qPCR. N=3 biological replicates, statistical analysis performed using Student's T test. (**F**) Tumor volume in male (left) and female (right) WT and M-BKO mice. 300,000 B16-F10 cells were injected subcutaneously in the right flank. N= 18 (male) and 8 (female) mice, statistical analysis performed using 2-way ANOVA for WT vs. M-BKO mice across the time course. (**H**) Gene expression for F4/80^{+} cells isolated from B16-F10 tumors or spleens of female mice 14 days after injection. Tissues from 6 mice per genotype were pooled into 3 groups for leukocyte isolation. Statistical analysis performed using Student's T test. Data presented as mean ± S.E.M. *p<0.05. Experiments were repeated at least twice.
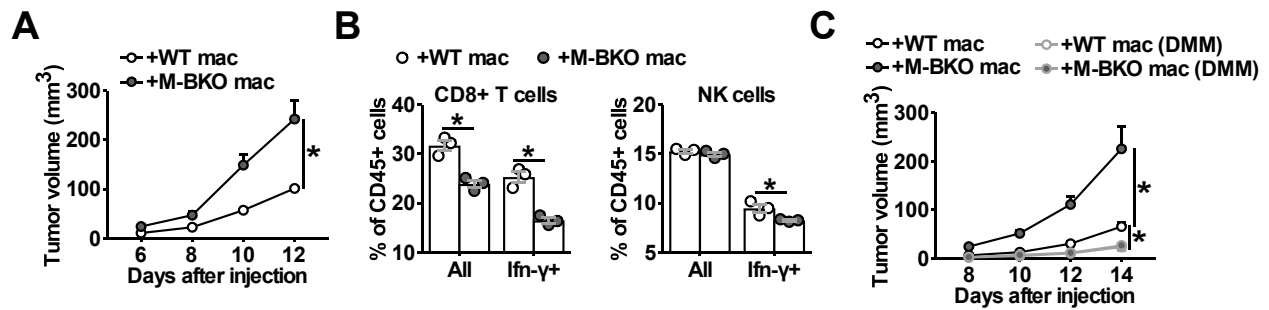
Figure 7. Macrophage Bmal1 modulates the antitumor activity.
(**A**) Tumor volume in WT male mice co-injected with 500,000 B16-F10 cells and either 500,000 WT or M-BKO macrophages as indicated. N= 22 mice, statistical analysis performed using 2-way ANOVA for WT vs. M-BKO macrophage co-injection across the time course. (**B**) Flow cytometric analysis of tumor-infiltrating CD8+ T cells (CD45+CD3+CD8a+ cells, left panel) and NK cells (CD45+CD3-NK1.1+ cells, right panel) stimulated *ex vivo* with phorbol 12-myristate 13-acetate and ionomycin for Ifn-γ co-staining. Tumors from (A) were pooled into three groups prior to isolation of infiltrating leukocytes for flow cytometry. Statistical analysis performed using Student's T test. (**C**) Tumor volume in WT male mice co-injected with 500,000 B16-F10 cells and either 500,000 WT or M-BKO macrophages supplemented without or with dimethylmalonate (DMM, approximately 150 mg/kg body weight per day in mouse diet). N=8 mice, statistical analysis performed using 2-way ANOVA for WT vs. M-BKO macrophage co-injection on control diet or for WT macrophage co-injection on the control diet vs. WT or M-BKO macrophage co-injection on the DMM-supplemented diet across the time course. Data presented as mean ± S.E.M. *p<0.05. Experiments were repeated at least twice.
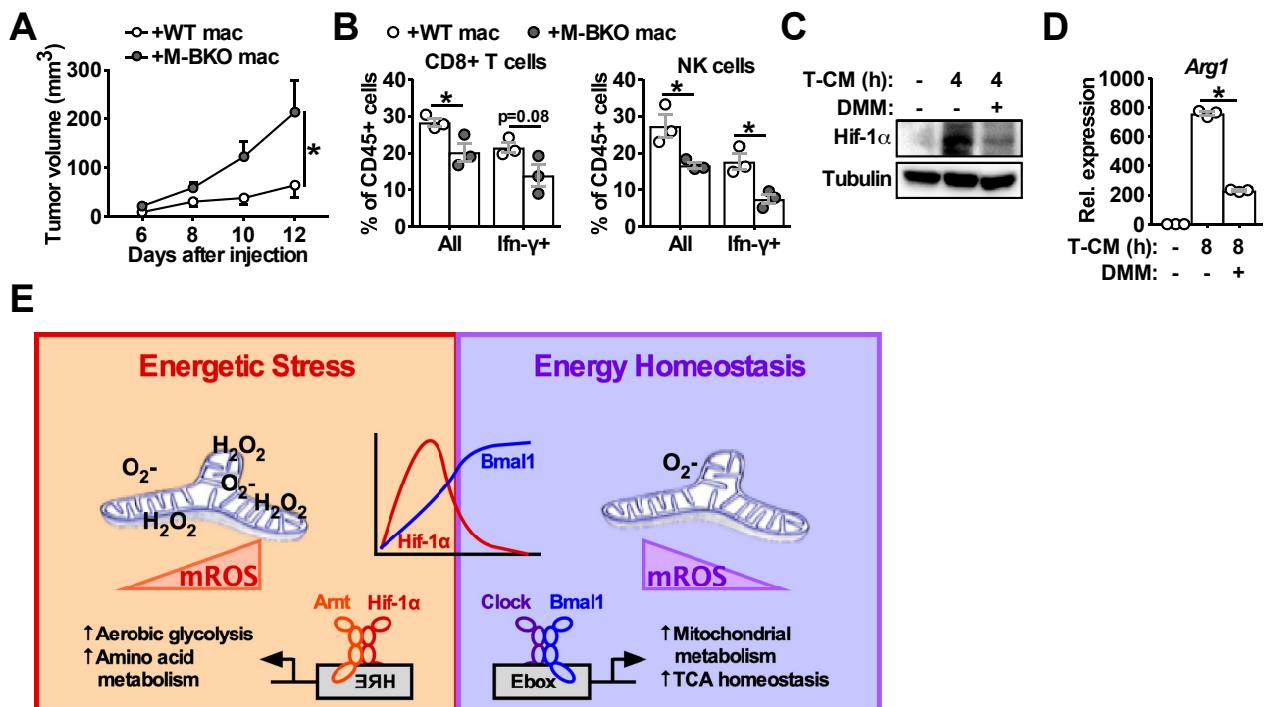
Figure 7 supplemental figure 1. Macrophage Bmal1 regulates tumor growth in a cell-autonomous manner.

(**A**) Tumor volume in M-BKO male mice co-injected with 500,000 B16-F10 cells and either 500,000 WT or M-BKO macrophages as indicated. N=6 mice, statistical analysis performed using 2-way ANOVA for WT vs. M-BKO macrophage co-injection across the time course. (**B**) Flow cytometric analyses of tumor-infiltrating CD8$^+$ T cells (CD45$^+$CD3$^+$CD8a$^+$ cells, left panel) and NK cells (CD45$^+$CD3$^-$NK1.1$^+$ cells, right panel) stimulated *ex vivo* with phorbol 12-myristate 13-acetate and ionomycin for Ifn-γ co-staining. Tumors from (A) were pooled into three groups prior to isolation of infiltrating leukocytes for flow cytometric analyses. Statistical analysis performed using Student's T test. Data presented as mean ± S.E.M. *p<0.05. (**C**) Hif-1α protein levels in WT macrophages treated with (from left to right) control medium or B16-F10 tumor-conditioned medium (T-CM) diluted 1:1 with control medium without or with co-treatment with 10 mM dimethyl malonate (DMM) for 4 hours. (**D**) *Arg1* gene expression in WT macrophages treated as in (C) for 8 hours. N=3 biological replicates. Statistical analysis performed using Student's T test. Experiments were repeated at least twice. (**E**) Schematic showing the working model for Bmal1-Hif-1α crosstalk in the regulation of macrophage bioenergetics and effector functions. Both M1 and tumor-associated macrophages share similar energetically stressed states. Bmal1 preserves mitochondrial oxidative metabolism while reducing oxidative stress to modulate Hif-1α activity and support proper effector functions. Deletion of *Bmal1* in the macrophage leads to reliance on glycolytic metabolism and alternative fuel utilization, notably amino acid metabolism, which further promotes mROS production and Hif-1α protein stabilization. Increased amino acid utilization by M-BKO macrophages may lead to depletion of amino acids critical for lymphocyte activation and cytotoxic function, thereby suppressing anti-tumor immunity in the tumor microenvironment.